



# Greening to shield: The impacts of extreme rainfall on economic activity in Latin American cities

Rafael Van der Borgh<sup>\*</sup>, Montserrat Pallares-Barbera

Universitat Autònoma de Barcelona, Departament of Geography, Barcelona, Spain

## ARTICLE INFO

### Keywords:

Climate risk  
Nature-based solutions  
Urban resilience  
Flood-related losses

## ABSTRACT

Latin American cities are increasingly impacted by floods and this trend is likely to be further exacerbated under the combined effects of climate change and urbanisation. To reduce urban flood risk, green infrastructure and the ability to preserve and rehabilitate green spaces is often mentioned as an option to improve the hydraulic response of cities. Yet, little empirical evidence exists about the degree to which a greener city land cover can reduce the impacts of extreme rainfall on urban economic activity. Using earth observations from 630 cities across Latin America, this paper shows that extreme rainfall has a negative impact on urban economic activity, as proxied by cities' night lights. Importantly, it finds that this negative impact diminishes as city's land cover becomes greener: for cities where dense vegetation represents more than 20 % of total city area, the marginal impact of extreme rainfall is broadly halved vis-a-vis cities below this threshold. A counterfactual analysis for the year 2015 suggests that increasing the greenness of 25 % of the cities in our sample could have reduced losses by US\$ 6,500 million -equivalent to a 19 % reduction of total estimated losses. These results evidence the benefits that a greener city land cover that makes room for green infrastructure can provide to adapt to more erratic rainfall patterns.

## 1. Introduction

In Latin America, both the frequency and damage associated with floods have been on an upward trend. While, on average, four floods per year were reported during the 1960s, this number has been steeply rising, reaching 13.8 floods per year during the 2010s and more than 22 per year during the first years of the 2020s (CRED, 2015, Fig. 1). Reported flood damages have multiplied almost seven-fold, to reach an average of US\$ 1,726 million per year during the 2010s (US\$ 2022, adjusted). Although these trends have mainly been driven by a steady expansion of population and assets into flood-prone areas (Jongman et al., 2012), local flood impacts display considerable variations across locations. Flood risk is in fact the product of a complex set of interactions between hazards (extreme rainfall), exposure (the presence of assets and persons in flood prone areas), and vulnerability (flood protection infrastructure, soil infiltration capacity – among other factors that influence the capacity to deal with extreme rainfall) (UNDRR, 2017).

In most cities of the region, this rising exposure to flooding has combined with a dramatic expansion of impervious soil surfaces, magnifying the impacts of extreme rainfall events. Hydrological

literature has extensively evidenced that the expansion of impervious surfaces alters the rainfall-runoff process (Yao et al., 2016, Jacobson, 2011, Mejía and Moglen, 2010, Arnold and Gibbons, 1996, among others). In short, impervious soil interferes with the natural process of water infiltration and increases both the velocity and volume of surface run off, exacerbating the magnitude of urban flooding when adequate drainage systems are not in place. Looking forward, urbanisation is anticipated to continue across central and south America, which could deepen this soil-sealing process and increase the extent of urban areas exposed to flood in the region by a factor 3.2 by 2030 (Güneralp et al., 2015).

Simultaneously, the hydrological cycle is expected to continue intensifying as the climate warms, resulting in more frequent extreme precipitation events, particularly in wet regions (Tabari, 2020). Projections from 33 models included under the CMIP-6, converge on the conclusions that maximum 5-day precipitation will increase for all Latin American sub-regions except South-Western America (IPCC, 2023).<sup>1</sup> Under the combined effects of urbanisation and climate trends, flood impacts are likely to be further aggravated, in particular in urban centers and their surrounding areas (Dottori et al., 2018; Steinhausen et al., 2022).

<sup>\*</sup> Corresponding author.

E-mail addresses: [rafael.vanderborgh@autonoma.cat](mailto:rafael.vanderborgh@autonoma.cat) (R. Van der Borgh), [montserrat.pallares@uab.cat](mailto:montserrat.pallares@uab.cat) (M. Pallares-Barbera).

<sup>1</sup> The magnitude of this increase is heterogeneous across regions: median estimates for the end of the century under high-warming scenarios (i.e. RCP 8.5) suggest an increase that could reach 23.8% for the South-East America region or only 4.8% for South Central America.

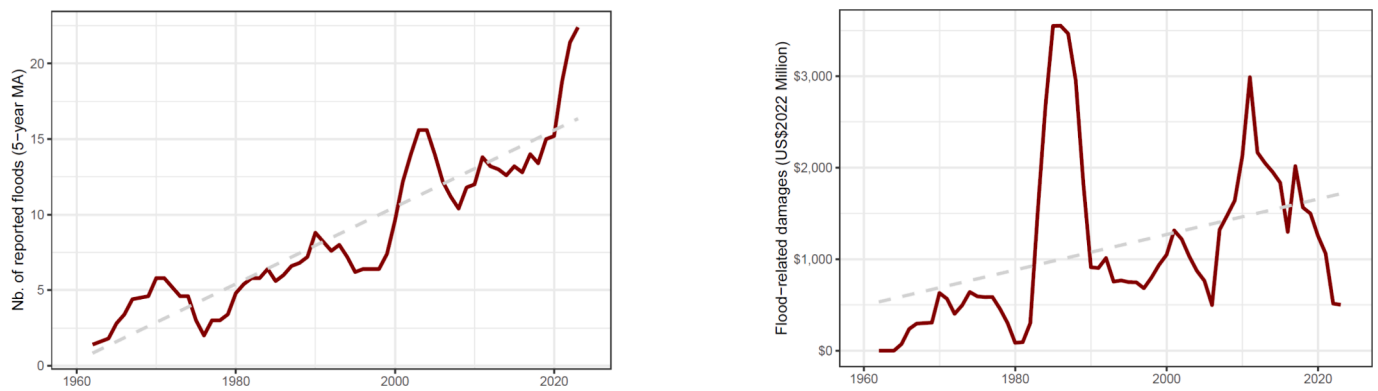


Fig. 1. Flood frequency and damage in Latin America: 1965–2022 (5 year moving average).

In order to confront these growing risks, green infrastructures (GI) for flood protection have received increasing attention.<sup>2</sup> Traditional urban flood control infrastructure, such as dykes, drainage networks or channels, can efficiently drain storm water out of the city. However, they entail important upfront capital costs and are complex to maintain in urban contexts characterised by poor solid waste management capacities (Lamond et al., 2012). They also display a finite water transport capacity, requiring costly upgrades in case of fast-paced urban growth and changes to precipitation patterns, to avoid quick saturation in the case of storm events (Schmitt et al., 2004). GI, on their hand, constitute a set of alternative interventions that seek to bring hydrological responses closer to pre-urbanised conditions by enhancing water infiltration capacity. GI which addresses pluvial flooding typically includes rain gardens, infiltration trenches, bio-swales or permeable pavements, which are capable of significantly reducing and postponing peak runoff, thus limiting the downstream flooded area for a given extreme rainfall event (Schubert et al., 2017). Likewise, interventions to reduce the impact of fluvial flooding can range from localized streambed re-naturalisation to more ambitious re-meandering and restoring upstream floodplains or wetlands. Interventions to address fluvial flood risk usually imply important coordination works but deliver high flood protection benefits (Gourvitch et al., 2020). Importantly, all GI deliver additional co-benefits by providing multiple ecosystems services ranging from aesthetic value and recreational opportunities to biodiversity conservation, temperature regulation and carbon sequestration (Brink et al., 2016).

Despite this growing interest, properly quantifying the value of GI remains a challenging task notably because little is known about the benefits of GI in terms of protecting assets and reducing economic disruption triggered by extreme rainfall events. Bhattacharjee and Behera (2018) have for example provided evidence of a negative association between forest cover and flood impacts in terms of death and population affected in India but have not examined the economic effects of forest cover in case of flood. In the specific context of urban areas, hydrological modelling analysis indicates that GI deliver non-linear effects, with a highly heterogeneous relationship between imperviousness changes and rainfall-runoff alterations (Anni et al., 2020, Yang et al., 2015, Yao et al., 2016, Schubert et al., 2017). GI also display saturation effects once the infiltration capacity of the existing GI is exceeded (Ellison et al., 2017). Besides, detailed flood risk simulations for Shanghai have highlighted that GI can play a critical role, although on their own, they cannot maintain future flood risk at a low level (Du et al., 2020). More generally, flood risk reduction measures, including GI schemes, are rarely monitored and available assessments have predominately focused on high-income countries (Poussin et al., 2015).

As a result, for most intermediate and small cities in Latin America,

there is very little empirical evidence that determines the extent to which GI can reduce the effects of extreme rainfall on urban economic activity. Yet, GI could be particularly attractive to Latin American cities, which often display insufficient traditional flood control infrastructure and face complex maintenance challenges. The prospects of rising urban flood risk throughout the region only reinforce the urgent need to quantify the potential benefits associated with these interventions. This knowledge gap also contrasts with the mounting evidence that indicates that GI help reducing local temperature and the adverse impacts associated with Urban Heat Island effects (Iungman et al., 2023).

To fill this knowledge gap, this study leverages the rapidly growing literature that uses night-time light (NTL) satellite imagery to evaluate the impacts of extreme rainfall or other disasters on local economic activity (del Valle et al., 2020, Kocornik-Mina et al., 2020, Mohan and Strobl, 2017, among others). Since the work of Chen and Nordhaus (2011), night-time lights have been increasingly used as a proxy for economic activity. This source of data has proven particularly useful when studying the variations of local economic activity in urban areas (Gibson et al., 2021). Cities affected by extreme rainfall may experience power outages, damage to streetlights infrastructure or even evacuation that lead to reduced or altered city night-light patterns. These changes in light intensity and distribution provide quantitative insights into the severity and duration of extreme rainfall impacts that can be used to proxy variations in local economic activity. Inspired by this literature, this paper estimates (i) whether and to what extent extreme rainfall impact city NTLs and (ii) how a greener land cover in a city can change this relationship. Intuitively, because greener land cover can facilitate rainfall absorption, it is expected that cities with a higher proportion of green areas will suffer less economic impacts than those where land cover is almost exclusively made of impervious surfaces.

To empirically test this hypothesis, an internationally harmonised definition of cities is employed to delineate 630 cities across seven Latin American countries (i.e. Argentina, Brazil, Colombia, Chile, Ecuador, Mexico and Peru). Earth observations are then leveraged over the period 2013–2021, to gather key information on (i) rainfall patterns, (ii) urban economic activity, proxied through monthly night-time lights and (iii) impervious land cover features using NDVI composites. Eventually, fixed effect econometrics are used to assess the causal relationship between extreme rainfall and NTL and examine how the greenness of city land cover can act as a mediating factor.

Our results fall into three broad categories. This paper first contributes to the climate economy literature by documenting how extreme rainfall triggers negative and significant impacts on NTL at the city level, with the mean extreme rainfall event estimated to reduce NTL/cap by 17.9%. Second, findings reveal that this negative impact diminishes as city land cover becomes greener; for cities where dense vegetation represents more than 20% of total city area, the marginal impact of extreme rainfall is broadly halved vis-a-vis cities below this threshold. Eventually, the most important contribution of this paper relies upon the

<sup>2</sup> Green infrastructures go beyond flood protection measures but, for the sake of conciseness in this investigation, it was decided to restrict it to flooding.

proposed valuation of the benefits that greener land cover could bring in terms of avoided losses. This valuation is conducted by simulating an increase of the greenness index in 25 % of the cities in our sample. Leveraging the correlation between NTL and GDP, avoided NTL losses under this simulated scenario are translated into monetary values. It is suggested that, in 2015 alone, losses could have been reduced by approximately US\$ 6,500 million (2015 constant), which is roughly equivalent to a 19 % reduction of observed losses.

The remainder of this paper is structured as follows: Section 2 details the methodology employed to assemble our panel. Section 3 presents the empirical framework used to assess the relationship between extreme rainfall and NTL and explore the heterogeneity of impacts associated with different levels of greenness. Section 4 documents the results of this assessment and simulates the losses that could be avoided if selected cities increased the greenness of their land cover. The last section discusses these results and concludes.

## 2. Methods and materials

In this paper, cities are defined in a systematic way across the seven countries of interest, using the degree of urbanisation concept (Dijkstra et al., 2020). According to this methodology, urban centres are population clusters that meet two criteria: a minimum density of 1,500 people per km<sup>2</sup> and a total population of at least 50,000 inhabitants. To ensure replicability, this analysis used the extents of urban centres provided by the Urban Centre Database (UCDB available here; see Florczyk et al., 2019 for a full description). This population-based approach is more likely to depict the socio-economic reality and spatial extent of the urban system than administrative boundaries (Van der Borgh and Pallares-Barbera, 2023). The final sample we used in this investigation included 630 cities, ranging from small urban areas (50,000 people, as per the definition of the degree of urbanisation) to giant megalopolises (almost 20 million people for Mexico City or Sao Paulo, see Map 1 in Appendix A).<sup>3</sup> Importantly, it covered the spectrum of small and intermediate cities that make up the bulk of the urban system, providing a comprehensive view of human settlements: half of the cities in our sample had a population below 107,000 in 2015 and only 37 cities had a population of over a million. Taking advantage of the spatial nature of this city database, we then overlaid this ‘city layer’ with earth observations, to gather the three main variables of interest at the city level, namely: rainfall, night-time lights (NTL) and greenness of the land cover.<sup>4</sup>

### 2.1. Precipitation and extreme rainfall events

Precipitation data was extracted from the CHIRPS pentad product (Funk et al., 2015) at a spatial resolution of 0.05°. City-level precipitation was computed based on a zonal sum of the CHIRPS pixels intersecting with city extents. Following standard climatological practices, which use a minimum of 30 years to define ‘climate normal’, the 5-days precipitation data was aggregated on a monthly basis over the period 1991–2021 (WMO, 2023). To be able to accurately capture extreme rainfall events across different climatological areas, we normalised precipitation on a city-monthly basis using the traditional Z-score formula described in Eq. (1).

$$Z_{m,j} = \frac{X_{m,j} - \bar{X}_{m,j}}{\sqrt{\frac{1}{M} \sum_M (X_{m,j} - \bar{X}_{m,j})^2}} \quad (1)$$

<sup>3</sup> To avoid measurement errors, we focused on cities with over 50,000 inhabitants in 2015 and manually removed the following observations: 2 potentially false positive urban centers, 11 cities with missing temperature data and 22 cities with, on average, less than 3 days of cloud-free observations per month.

<sup>4</sup> The overlay and zonal operations described hereafter were performed through the Google Earth Engine (GEE).

$$\text{Extreme rainfall}_{m,j} = \begin{cases} Z_{m,j}, & \text{if } Z > 2 \text{ and } \bar{X}_{m,j} > 30 \\ 0, & \text{otherwise} \end{cases} \quad (2)$$

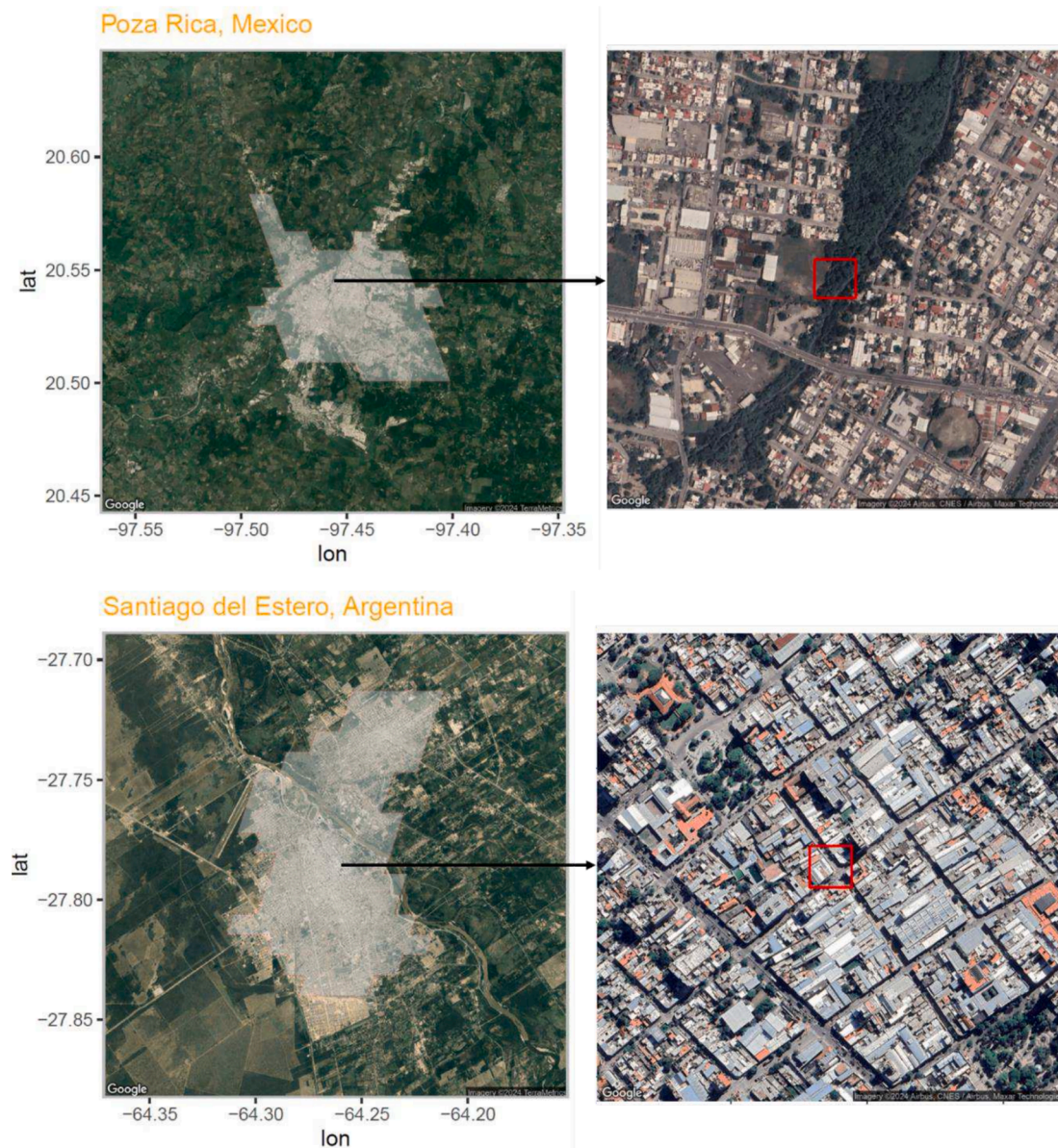
$X_{m,j}$  is the monthly precipitation in month  $m$  in city  $j$  and  $Z_{m,j}$  is the Z-score of this precipitation relative to its mean and standard deviation over the period 1991–2021. By normalising precipitation data, we obtained a measure that is comparable across geographies. Our extreme rainfall index was then computed following a double condition: first, the Z-score should be above 2 (i.e. monthly precipitation is two standard deviations above the mean precipitation); second, absolute monthly precipitation must exceed 30 mm, to ensure that only extreme rainfall events occurring during a rainy month are retained (Eq. (2)). This double condition allowed us to focus on months where soil infiltration capacity was more likely to be saturated and where extreme rainfall was, therefore, more likely to trigger damaging floods. With this definition, extreme rainfall events constituted less than 3 % of total precipitation observations over the period, which is consistent with WMO recommendations, which considers extreme rainfall events to be those events whose ‘occurrence tends to take the form of the upper 90th, 95th and 99th percentile of precipitation’ (WMO, 2023). To test the robustness of our approach, two alternative precipitation indexes were used: the first was based on the full range of precipitation Z-score values; the second was based exclusively on a positive Z-score and accounted for a month where a city experiences precipitation above its mean value.

We repeated the same process for temperature data, which is potentially correlated with precipitation.<sup>5</sup> Temperature data was extracted from the ERA-5-Land product provided by the Copernicus Climate Change Service (C3S) at a 0.1° resolution. The value of pixels intersecting with city extents was extracted and averaged by area before being normalised using the same Z-score formula as for precipitation. Temperature deviations were used as a control variable, exclusively, and we refrained from a causal interpretation, as the conceptual relationship between temperature anomalies and night-time light remains unclear.

It is important to underscore that this paper deliberately rejected the use of data on flood-related impacts as an explanatory variable because of endogeneity concerns. Data on flood impacts may correlate with development levels and, therefore, with city-level NTLs (i.e. our dependant variable). Indeed, data on the impact of flooding is, by essence, an endogenous variable: damage caused by urban flooding are functions of the vulnerability levels of the affected area which, in turn, depend on the level of economic development of those areas (see Felbermayr et al. (2022) for a more detailed discussion). To address this reverse causation issue, we propose the three above-mentioned precipitation indexes, which have the advantage of being exogenous to economic development and are preferred in our identification strategy. However, precipitation indexes are not intended to be a perfect predictor of flooding. In fact, in urban contexts, at a fine spatiotemporal resolution, extreme precipitation events and floods are unlikely to occur at the exact same location and at the same moment.<sup>6</sup> In this investigation, we intentionally worked at a relatively low spatiotemporal resolution, to minimise the potential mismatch between extreme rainfall events and floods (i.e. city-monthly level as opposed to pixel/daily level).

<sup>5</sup> The Clausius-Clapeyron relation suggest that, for every 1°C of increased air temperature, the water-holding capacity of the atmosphere rises by about 7%. More moisture is therefore available in a warmer atmosphere than in a colder one, creating heavier rainfall when precipitation forms. As temperature and precipitation can both affect economic activity, the exclusion of temperatures could bias our estimates.

<sup>6</sup> The location and spatial extent of flooded areas are influenced by local factors such as topography, soil infiltration capacity and drainage systems capacity, among others. These factors channel water runoff away from the location where the rainfall has occurred, generating a ‘spatial lag’ between the location of extreme rainfall and flooded areas. Likewise, flooding only materialises after a significant amount of rainfall, generating a ‘temporal lag’ between peak precipitation moment and flooding.



**Map 1.** Visual comparison of two cities displaying differentiated greenness indexes. *Note:* The left panel maps the extent of each city according to the UCDB. The right panel zoom-in on the centre of each map to provide an illustration of vegetation cover. The red squares represent a 30 m pixel. Source: Google Maps

## 2.2. Nighttime lights and urban economic activity

The literature using nighttime lights to proxy economic activity in small geographic areas has relied on two major datasets. The Defense Meteorological Satellite Program (DMSP) satellites, with a spatial resolution of approximately 1 km and an annual coverage over the period 1992–2013, have been extensively used to assess the impacts of large-scale natural disasters (Klomp, 2016), weather anomalies (Felbermayr et al., 2022) or to quantify the impacts of extreme precipitation and floods (del Valle et al., 2020, Kocornik-Mina et al., 2020). More recently, the release of the Visible Infrared Imaging Radiometer Suite (VIIRS) instrument has provided a newer source of NTL data with a finer spatial resolution (approximately 450 m at the equator) and a monthly coverage from April 2012 to the present (contemporaneous observations are generally issued with a 4-month lag; see Elvidge et al. (2017) for a description of VIIRS). This dataset has also been used to (i) proxy local economic activity (Chen and Nordhaus, 2015, Zhao et al., 2017) or (ii) detect damages and power outages in the aftermath of flood events (Zhao et al., 2018, Levin and Phinn, 2022) and hurricanes strikes

(Mohan and Strobl, 2017).

As evidenced by Gibson et al. (2021), the VIIRS dataset is more suitable than the DMSP one to proxy economic activity at city-level. This is primarily due to the top-coding feature of the DMSP, which understates the intensity of lights in brightly lit city centers.<sup>7</sup> Additionally, the monthly frequency of this NTL data source is crucial for capturing relatively short-term disruptions, such as those triggered by urban floods, which could be ‘averaged out’ when using annual observations provided by the DMSP product.

Given the above, this study uses the VIIRS NTL dataset to proxy economic activity at the city-level. Specifically, we refer to urban economic activity as the zonal summation of NTL pixels located within city

<sup>7</sup> The DMSP measures NTL intensity using a Digital Number ranging from 0 to 63. While city centers pixels typically register the maximum value of 63, other regions like suburbs or smaller towns also saturate DMSP sensors, resulting in the same number and lessening distinctions in light intensity among areas. VIIRS sensors offer a broader range and do not show saturation problems.

extents. Following [Elvidge et al. \(2017\)](#), we cleaned the dataset from very low cloud-free coverage observations, by removing 22 cities that, on average, had less than 3 days of cloud-free observations per month, over the period considered. To address the airglow issue noted by [Upreti et al. \(2017\)](#), we manually set negative NTL values to '0', which represented 0.1 % of total observations.<sup>8</sup> We then restricted our sample to cities that have experienced at least one extreme rainfall event during the period 2013–2021. The final panel comprised 630 cities observed over 108 months (i.e. 9 full years).

Intuitively, one would expect city-level NTLs to experience a reduction in the aftermath of an extreme precipitation event. It is important to underscore that this reduction in NTL values can be associated with power outages and/or damages and direct destruction of city light infrastructure, which represent two very different economic impacts in nature: one denotes a destruction of physical and productive assets, and the other is associated with disruption and losses linked to interrupted activities or foregone revenues. Although it is impossible to distinguish between these two effects with NTL data, capturing both effects is fully relevant to provide a comprehensive view of the impacts of extreme rainfall on urban economic activity.

A quick visual examination of different cities experiencing extreme precipitation events, and for which a flood had been reported, seems to confirm the expected pattern ([Fig. 2](#)). According to [Brakenridge \(2023\)](#), the city of Governador Valadares (in Brazil) experienced flooding from 23rd December 2013 to the first weeks of January 2014, and displayed a significant reduction of NTL/capita in the following months. In the case of Santiago (in Chile), the flood reported from the 15th to the 18th April 2016 seemed to have exacerbated a drop in NTLs that started before the flood. Interestingly, for Santiago, two other extreme precipitation events were detected during the two-year period of this visual analysis and seem to have also been accompanied by a drop of NTLs. Overall, for both cities, NTL/capita reached their lowest level over a two-year period in the aftermath of the reported flood. Although the high volatility of NTL/capita makes it difficult to isolate the effects of extreme precipitation from other variations, this visual examination constitutes suggestive evidence that extreme precipitation could result in a deviation of NTL/cap from baseline trends.

The statistical analysis in the next sections robustly assesses whether NTLs deviate from their trend in the case of an extreme rainfall event and properly quantify this effect by isolating it from other factors. One important concern is however linked to the reduction of cloud-free observations during the months where an extreme precipitation event is detected. With a Pearson's coefficient estimated at 0.32, the correlation between the number of cloud-free observations and NTL values warrants a cautious approach (see [Appendix C](#)). The observed reduction in NTL values during months of high cloud-coverage could confound the estimation of extreme rainfall impacts, as NTL reduction presumably linked to damage or power outages could, in fact, be driven by higher cloud-coverage. While we cannot fully isolate variations in NTL values due to higher cloud-coverage from factors linked to power outages and damage to infrastructure, we argue that if the monthly variation linked to cloud-coverage commonly impacts all cities within a given area, it can be at least partially captured by a country-monthly fixed effect (see [Appendix C](#) for more details).

### 2.3. City land cover and greenness index

The number of satellite-derived land cover products has been rapidly growing during the last decade, although these products differ signifi-

cantly, in terms of spatiotemporal resolution and scale. Of the existing products, Landsat imagery has proved to be the one of the best data sources, accurately capturing land cover features at a global level ([Sun et al., 2022](#)). Consequently, to proxy vegetation cover this study leverages annual NDVI composites from the Landsat 8 Collection 1 Tier 1 orthorectified scenes, using the computed top-of-atmosphere (TOA) reflectance. NDVI pixels have a 30-meter resolution and, following usual practice in land cover analysis, we consider that pixels with a value above 0.5 are associated with dense vegetation, such as trees, urban gardens or parks or even urban forests. We therefore computed the annual share of pixels with a value above 0.5 for each city in our sample over the period 2013–2021. To mitigate inter-annual variability, we use the mean value of this annual share over the period and express our greenness index through the ratio of dense vegetation areas within the city relative to the total city area, as shown in [Eq. \(3\)](#) below.

$$\text{Greenness index}_j = \frac{\text{Dense vegetation areas}(\text{NDVI} > 0.5)_j}{\text{Total city area}_j} \quad (3)$$

We conducted a quick visual comparison of different cities through Google maps satellite imagery (i.e. a different data source than the one used to compute NDVIs). [Map 1](#) shows the cities of Poza Rica, Mexico and Santiago del Estero, Argentina, which display a greenness index of 27.8 and 6.5, respectively. Randomly zooming within city borders confirmed a more prominent presence of dense vegetation in Poza Rica, which is consistent with a higher value of the greenness index. To test the sensitivity of our results to different greenness measurement, we computed a more restrictive greenness index based on the share of NDVI pixels above 0.6 and used an alternative source of data to derive the greenness index (see [Appendix D](#)).

### 3. Calculation

The empirical analysis undertaken in this paper comprised a twofold approach. First, the relationship between extreme rainfall and NTL at the city level was investigated; then the heterogeneity of effects associated with extreme rainfall was explored by interacting the extreme rainfall index with the greenness index.

The empirical framework proposed in this paper directly drew from the approach proposed in the recent climate-economy literature ([Dell et al., 2014](#)). The assumption underpinning our identification strategy is that extreme rainfall events are exogenous and conditional on city and country-month fixed effects. Consequently, our benchmark model takes the following form:

$$\ln Y_{i,c,m} = \alpha + \beta_1 (Xtrm_{i,c,m}) + \beta_2 (Tmp_{i,c,m}) + \omega_i + \theta_{cm} + \varepsilon_{i,c,m} \quad (4)$$

$\ln Y_{i,c,m}$  represents the log-transformed value of NTL per-capita of city  $i$  in country  $c$  and month  $m$ .<sup>9</sup>  $Xtrm_{i,c,m}$  is the extreme rainfall index, as described in the previous section,  $Tmp_{i,c,m}$  is a vector of monthly temperature z-scores,  $\omega_i$  are city-fixed effects and  $\theta_{cm}$  are month-by-country fixed effects (i.e. monthly fixed-effects interacted with country dummies). The exclusion of temperature variables could imply a potential mis-specification bias although, in our setting, this variable is to be viewed as a control variable.  $\varepsilon_{i,c,m}$  is the robust error term, clustered by city.

With this model, we analysed whether city-specific NTL deviations are related to city-specific deviations from precipitation trends, after accounting for unobserved time-invariant heterogeneity, as well as monthly shocks, common to all cities in the country of interest.

<sup>8</sup> The underlying processes for constructing VIIRS NTL cleans the raw data captured by the satellite to remove noise and direct light from the moon or sun. This process is automated and follows a methodology where an amount is deducted from the raw value of the lights. This process is sometimes affected by airglow and deducts an amount exceeding the value of captured light, resulting in negative NTL values.

<sup>9</sup> City NTL per-capita were estimated using the 2015 city population estimates provided in the UCDB. We added 0.001 to all city NTL values before log-transforming them, to avoid removing observations where monthly NTL values were 0. We tested and rejected the null hypothesis of the presence of a unit root in our dependent variable.

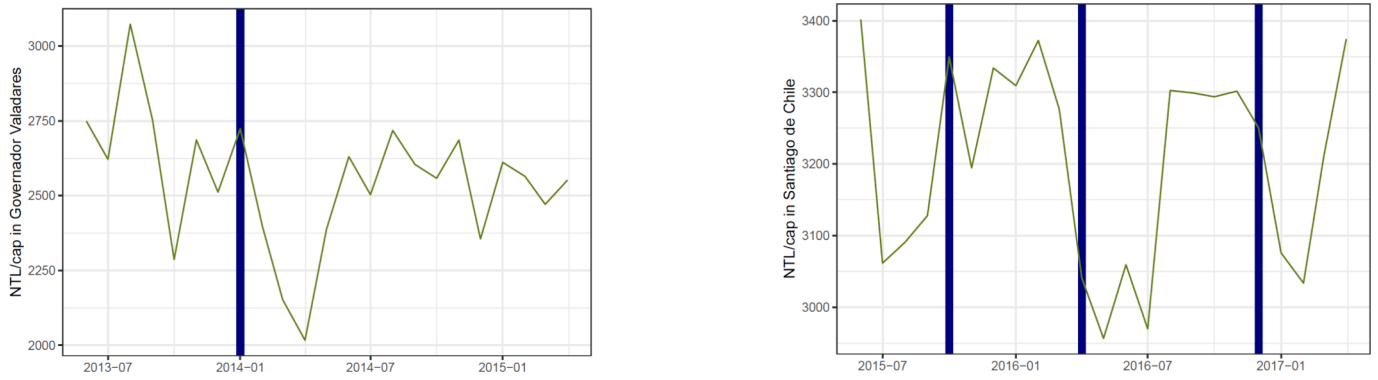


**Fig. 2.** VIIRS Nightlights in Governor Valadares, Brazil (left) and Santiago, Chile (right) before and after extreme rainfall events. *Note:* the blue bar denotes the occurrence of an extreme rainfall event. (For interpretation of the references to colour in this figure legend, the reader is referred to the web version of this article.)

Contextual effects that are, for example, associated with topography, elevation or culture are soaked up by city fixed effects, while changes in satellite imagery quality or international prices variations are subsumed into the monthly-country fixed effects.<sup>10</sup> This framework is well-suited to isolate the causal effect of extreme rainfall on NTLs.

The second step of our analysis investigates the effects of greener urban land cover by testing whether the impact of extreme rainfall on NTL decreases as the level of vegetation cover increases, everything else being equal. To ensure that these effects are not driven by an intrinsically higher vulnerability to extreme rainfall in cities where dense vegetation is inexistent, in this part of the analysis we removed cities that display no or very limited dense vegetation.<sup>11</sup> Cities with less than 5 % of their total area covered by high greenness pixels (i.e. approximately 20 % of our original sample) corresponding to urban centres with almost no trees nor dense vegetation are thus excluded of this analysis.

Because the hydrological literature has emphasised that there may be a non-linear relationship between the amount of GI and the observed reduction in urban flood extent (Schubert et al., 2017, Yao et al., 2016, Yang et al., 2015), we replicated the framework proposed by del Valle et al. (2019) and explored the heterogeneity of extreme rainfall effects by estimating three different models. For each model, we discretized the city greenness index into various bins, corresponding to different quantiles. The first model used the median value of the greenness index to create two dummy variables for each equal-sized bin and interact these dummies with the extreme rainfall index. The variable resulting from this interaction was then inserted into our benchmark equation, as shown in Eq. (5).

$$\ln Y_{i,c,m} = \alpha + \beta_1 (X_{trm_{i,c,m}}) + \beta_2 (X_{trm_{i,c,m}} \bullet \overline{\text{Green index}}_{i,c}) + \omega_i + \delta_{mc} + \varepsilon_{i,c,m} \tag{5}$$

The marginal impact of extreme rainfall in each bin was obtained by summing  $\beta_1$  and  $\beta_2$ . This procedure allowed the estimation of effects that vary in a non-linear fashion across bins, potentially capturing non-linearities in the impacts of extreme rainfall events across levels of greenness. We repeated this assessment discretizing the greenness index at the tercile and quarter values of the sample.

<sup>10</sup> To the extent that urban drainage systems have remained unchanged over the period of analysis, variations associated with this infrastructure are also soaked up by city fixed effects.

<sup>11</sup> This higher vulnerability could arise for example from the fact these cities are principally located in semi-arid areas with structurally lower soil infiltration rates. Removing cities that do not display abundant vegetation also ensures that the simulation conducted in the following section does not project an increase of the greenness index in cities that cannot accommodate dense vegetation because of strong water availability constraints.

When exploring the effects of the interactions between greenness index and extreme rainfall, we acknowledge that the greenness index could potentially be jointly determined with income per capita (proxied by NTL/cap) and precipitation patterns. To attenuate this issue, we used the average value of greenness over the period and ensured that city NTL/cap and greenness index did not change discontinuously at the threshold values selected, which could have potentially been driving the differentiated effects observed in each bin. As depicted in Fig. 3, there does not seem to be a clear relationship between greenness index and NTL/cap at the city level. With a Pearson coefficient of  $-0.06$ , the correlation between log-values of NTL/cap and the greenness index remains limited and is unlikely to explain the differentiated impacts of extreme rainfall events. We nonetheless refrained from claiming a causal interpretation of this effect.

## 4. Results

### 4.1. The effects of extreme rainfall on city-level NTL

The main results of estimating equation (4) with the data detailed in section 2 are presented in Table 1. A major finding of this first step was the systematic negative relationship between extreme rainfall and NTL/capita across Latin American cities. Column 1 shows the result of our benchmark specification and provides evidence that, on average, extreme rainfall has a negative and significant impact on city NTL/capita. To ensure the robustness of this estimation, we considered alternative rainfall proxies and a variety of robustness checks. Column 2 removes all other covariates and reveals similar impacts, corroborating the estimates obtained in column 1. Column 3 replaces the extreme rainfall index, with an index based exclusively on monthly precipitation above mean rainfall (i.e. Z score > 0) and finds consistently negative effects. Column 4 explores the presence of non-linearity in the relationship between NTL and precipitation, by replacing the extreme rainfall index by the full spectrum of precipitation values (normalised by the Z-score formula) along with its quadratic term but finds no evidence of it. Column 5 introduces precipitation Z score values in a linear fashion and confirms a negative relationship between rainfall deviations and city NTL/cap.

Temperature deviations show a consistent non-linear U-shaped effect on NTL/cap: positive temperature deviations raise the NTL/cap at first, although this effect is progressively reduced and, beyond a tipping point, reversed. Based on column 1, the tipping point for temperature Z score is estimated to be at 2.28, which is close to the maximum value recorded over the period (i.e. 2.8) and well above the third quarter of our temperature sample, indicating that negative temperature effects only prevail for a handful of cases.

Extensive robustness checks are presented in Appendix B. These indicate that these results are robust to the choice of fixed effects and

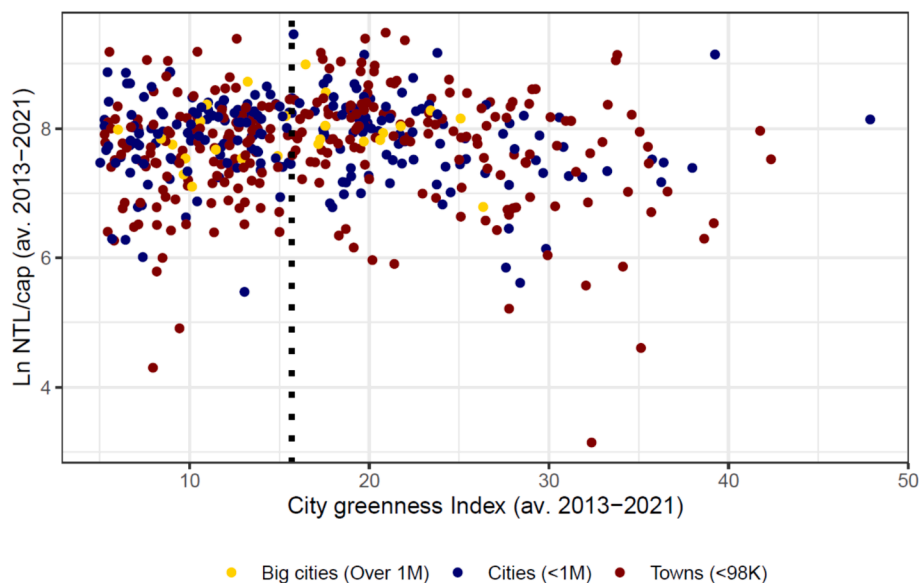


Fig. 3. Average city NTL/cap VS greenness index. Note: the dotted line represents the median of the greenness index.

Table 1  
Main estimation results.

	Dependent variable: Ln NTL/cap				
	(1)	(2)	(3)	(4)	(5)
Xtrm Rainfall	-0.069 <sup>***</sup> (0.014)	-0.076 <sup>***</sup> (0.014)			
Rainfall Zscore				-0.067 <sup>***</sup> (0.007)	-0.063 <sup>***</sup> (0.006)
Sq. Rainfall Zscore				0.004 (0.003)	
Temp. Z	0.058 <sup>***</sup> (0.007)			0.043 <sup>***</sup> (0.006)	0.044 <sup>***</sup> (0.006)
Sq. Temp. Z	-0.011 <sup>**</sup> (0.005)			-0.012 <sup>***</sup> (0.005)	-0.012 <sup>***</sup> (0.005)
Abov. mean rainfall			-0.088 <sup>***</sup> (0.009)		
Observations	68,040	68,040	68,040	68,040	68,040
F Statistic	57.1 <sup>***</sup> (df = 3; 66652)	73.6 <sup>***</sup> (df = 1; 66654)	184.6 <sup>***</sup> (df = 1; 66654)	70.8 <sup>***</sup> (df = 4; 66651)	93.9 <sup>***</sup> (df = 3; 66652)

Note: \*p < 0.1; \*\*p < 0.05; \*\*\*p < 0.01.

different computation of standards errors. Likewise, including cities that did not experience extreme rainfall events, or dropping the largest country of the region, did not change the significance of the coefficients. We further controlled potential cloud-coverage variations through more restrictive thresholds for cloud-coverage quality and additional seasonal trend controls, without finding evidence that this alters our results.

From a quantitative perspective, the results in column 1 indicate that, for Latin American cities, when an average extreme rainfall event occurs, the NTL/cap is reduced by 17.9 % (or -0.179 log points). This is obtained by multiplying our coefficient of interest by the average value of the extreme rainfall index (i.e. 2.5). Importantly, since extreme rainfall events are, by definition, rare events, we provide a probabilistic view of our estimates to better reflect the nature of impacts. In order to do this, we computed an empirical cumulative distribution function of the maximum extreme rainfall index, recorded annually, during the period 1991–2021, in each of the 630 cities. This procedure allows us to estimate the values of extreme rainfall index at different percentiles of the distribution and, consequently, to infer the annual probability of having a city exceeding a given extreme rainfall index. As such, until the 73rd percentile of the distribution, the value of the extreme rainfall index is 0, meaning that, across the seven countries of interest, the

annual probability of having at least one city experiencing an extreme rainfall event is approximately 27 % (1–0.73).

This probabilistic view reveals a non-linear relationship between extreme rainfall event realisations and NTL losses (Fig. 4). As such, the 80th percentile of the distribution corresponds to a value of 2.23, which implies that, at the regional level, there is a 20 % annual probability (1–0.8) of exceeding an extreme rainfall index of 2.23. In other words, the model predicts that, in the long run, Latin American cities face a 20 % annual probability of experiencing an extreme rainfall event that lowers monthly NTL per capita by approximately 15.4 % (i.e. 2.23 × 6.92). For extreme rainfall events displaying a 1 % annual probability of being exceeded, city NTL/cap is estimated to be reduced by 30.7 %. Worryingly, under the effects of climate change, future precipitation patterns are projected to significantly depart from the historical patterns used for this assessment. Events in the tail of the distribution (such as those with a 1 % annual probability) are expected to become more frequent, thereby increasing the likelihood of the region having to confront significant losses.

Finally, we need to understand whether negative impacts arising from extreme rainfall events produce: (i) permanent effects on a city's local economic activity, (ii) only a momentary impact, or (iii) are fully

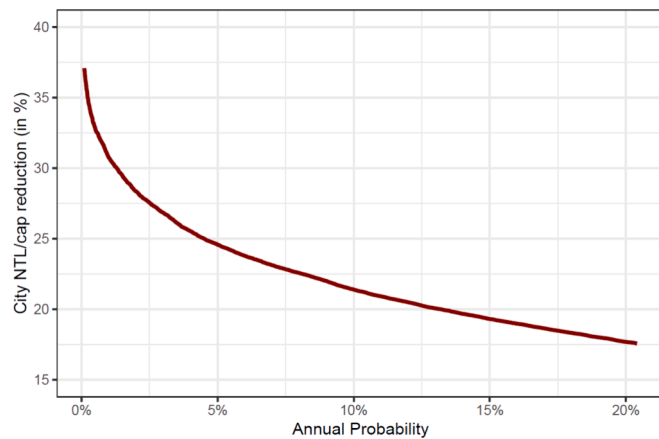


**Fig. 4.** Annual probability of exceeding a given city NTL/cap loss. *Note:* this figure was constructed using the empirical cumulative distribution of extreme rainfall events for 1991–2021 and the coefficient in column 1 of Table 1.

offset by a rebound in economic activity in subsequent months. Following Dell et al. (2014), we assessed these effects by including the monthly lagged values of the extreme rainfall index in Eq. (4). Fig. 5 plots the results presented in column 1 of Table B.3 in Appendix B; the contemporaneous effect of extreme rainfall is significantly negative and the first lag remains negative but no longer statistically different from 0 at the usual 5% threshold value. Subsequent extreme rainfall lags are hovering below and above 0 but are all statistically insignificant. A similar pattern is observed when using the index based only on positive Z scores. This suggests that the adverse economic effects of extreme rainfall are short-lived and, on average, do not persist after the month of impact. Insignificant lagged effects also point to the absence of economic rebound in the aftermath of extreme rainfall events.

#### 4.2. The greenness of the land cover as a moderating factor

We then proceeded to estimate the effects of a greener land cover through the three models indicated in section 3. Estimated effects are presented in Fig. 6(a), which plots the point estimates and 90% confidence intervals for each of the three models. The city and country-monthly fixed effects are included in the estimations. The coefficients can be interpreted as the marginal reduction in nightlights caused by an extreme rainfall event for each group of cities.

In the model with two bins, for cities below the median value of the greenness index (i.e. 15.69), the marginal extreme rainfall effect reduces nightlights by almost 12%. Contrastingly, in cities with greenness indexes above this median value, this marginal effect is reduced to approximately 5%. In addition, the null hypothesis of no differential impact of extreme rainfall events between the two bins was rejected ( $P$  value  $< 0.1$ ). Models with 3 and 4 bins show a consistently decreasing impact of extreme rainfall, as the level of greenness increases. In the case of the model using 4 bins, we were able to reject the null hypotheses of equality between the coefficients associated with the first and the fourth quartile ( $P$  value  $< 0.1$ ). For the model with 3 bins, we were not able to reject it at conventional levels and the reduction of extreme rainfall impact only seems to materialize in the third tercile (i.e. cities with greenness index above 19).<sup>12</sup> Fig. 6(b) plots the distribution of greenness index in each bin across these three models, unveiling how the impacts of excess rainfall are systematically and significantly lowered for bins displaying a greenness index that exceeds 20 (i.e. bins at the bottom of each figure).

<sup>12</sup> Estimating Eq. (5) using the third tercile of the greenness index (i.e. 19.70) to create 2 bins (i.e. above/below third tercile) allowed us to reject the null hypothesis of equality between the two coefficients.

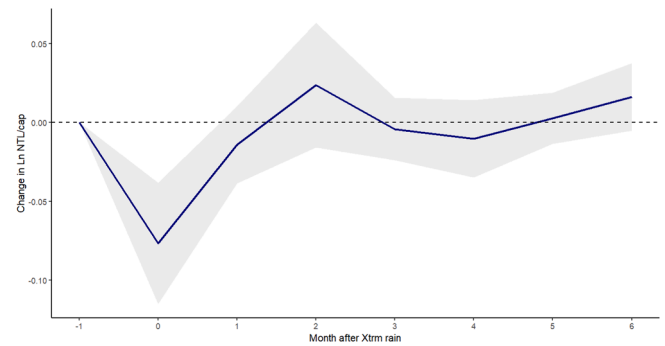


**Fig. 5.** Time dimension of extreme rainfall effects on city NTL/cap.

Extensive robustness checks were conducted in Appendix D and confirmed that results are not overly sensitive to (i) different NDVI or greenness index thresholds values (i.e. 0.5 or 0.6 to define dense vegetation pixels or varying the minimum value of the greenness index from 1 to 5 or removing potential outliers) or (ii) alternative spatiotemporal resolution to compute NDVI values. Ultimately, to ensure that results were not driven by other sources of heterogeneity potentially correlated to the greenness index, we performed three additional set of regressions allowing for extreme precipitation effects to vary based on greenness index and (i) total city population, (ii) average precipitation or (iii) city elevation. These regressions confirm that the reduction of impacts associated to a greener land cover remains significant and suggest that more populated cities in higher locations tend to be less vulnerable to extreme rainfall. Average precipitation levels do not seem to significantly influence extreme rainfall effects.

Altogether, results from these three models suggest that, for cities where dense vegetation represents more than 20% of total city area, the marginal impact of extreme rainfall is broadly halved vis-a-vis cities below this threshold. Consistent with the hydrological literature, in none of the models the adverse effects associated with extreme precipitation are totally wiped out by a greener land cover. This could be linked to soil infiltration saturation effects as well as the impossibility to maintain or expand green areas in some parts of the city. It also insinuates that GI alone might not be able to fully protect against the economic impacts of extreme rainfall. Significant protection benefits are nonetheless associated to a greener city land cover. According to our benchmark model (i.e. greenness index discretized based on its median value), the average extreme rainfall event observed over the period would lead to almost a 30% decrease in urban economic activity in cities where less than 15% of the area is associated with dense vegetation ( $2.5 \times -0.119$ ), while this reduction would be limited to approximately 14% in cities where green areas represent more than 15% of total city area ( $2.5 \times -0.055$ ).

#### 4.3. Valuation of the protection benefits associated with a greener city land cover

Finally, we leveraged the relationship between city NTLs and GDP to provide an economic valuation of the benefits associated with a higher greenness index, in terms of avoided losses. To this end, a simple calculation was performed using the benchmark model where cities are classified into two bins based on the median value of the greenness index. The computation was conducted for the year 2015 and followed three steps. First, city NTL variations were estimated by multiplying the extreme rainfall index recorded in each city by the coefficient corresponding to the greenness index of the city (either  $-0.055$  or  $-0.119$ ). Absolute NTL losses were derived by applying this variation to the 2015 mean city NTL/cap value and using the corresponding city population estimate. National NTL losses were obtained by summing all city NTL losses recorded in each country.

A counter-factual scenario was then simulated by computing NTL variations, under the hypothesis that cities displaying a greenness index

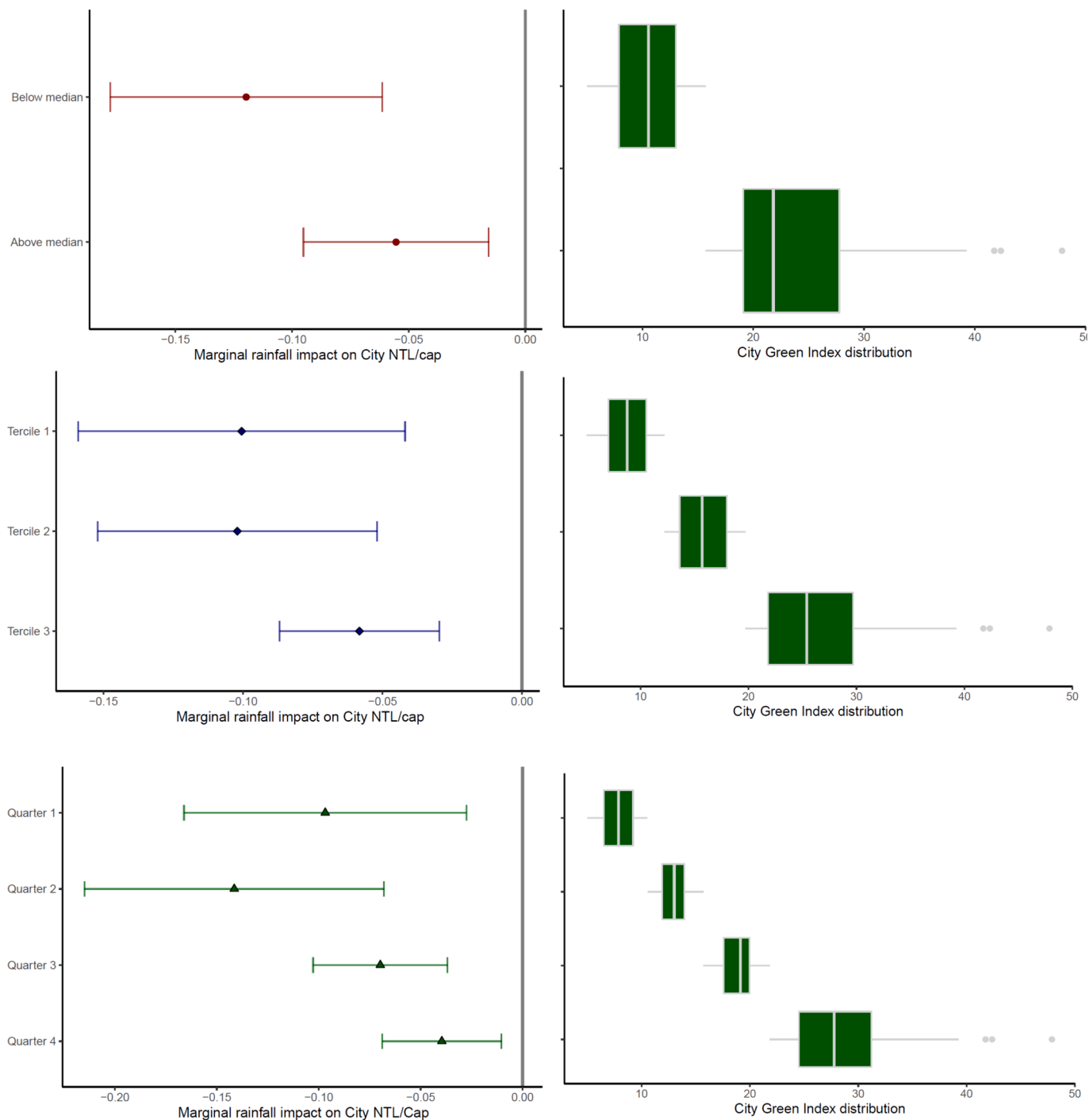


**Fig. 6.** (a) Estimated effects of three models of extreme rainfall interacting with q-quantiles of greenness index ( $q = 2$ ,  $q = 3$  and  $q = 4$ ; left). (b) Distribution of the greenness index in each group of cities (right).

between 10.52 (i.e. first quarter) and 15.69 (i.e. median value) increase their share of green areas. This ‘as-if’ analysis corresponds to a scenario where 25 % of the cities in our sample increase their average share of green land cover from the actual 13 % to close to 23 % (i.e. the mean value of greenness index in the bin above the median). To account for uncertainty in our estimates, this process was repeated 5000 times, drawing the coefficient associated with extreme rainfall from a normal distribution, which had the estimated parameter as its mean value and the estimated standard error as its standard deviation.

In the second step, we investigated the relationship between NTL and GDP to obtain a conversion factor between the two values. To this end, the annual mean city NTL values were summed at the national level and

regressed against the value of GDP (in constant US\$ of 2015). This regression did not seek to establish a causal relationship but attempted to provide a conversion factor between national city NTLs and GDP (see Appendix E for more details). To account for uncertainty, we used the same procedure as in the first step and repeated the translation of NTL to GDP values 5,000 times, drawing the coefficient of interest from a normal distribution, taking the estimated parameter as its mean value and the estimated standard error as its standard deviation. This procedure allowed us to translate the national NTL losses estimated in the first step into an equivalent variation of US\$. Thirdly, the benefits of greener city land cover were estimated as the difference between the mean ‘observed’ losses and the mean simulated losses under the ‘as-if’ scenario.

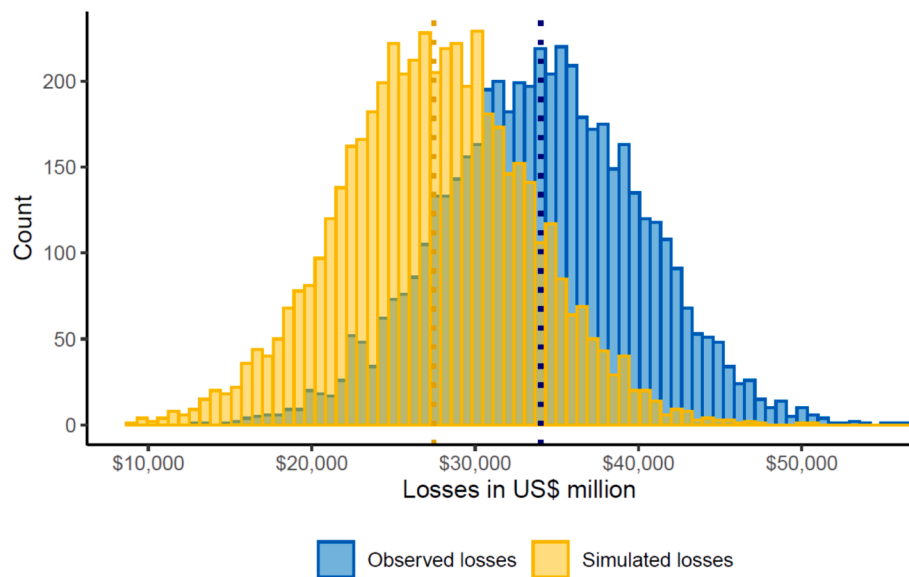


Fig. 7. Observed vs simulated losses based on 2015 extreme rainfall. Note: The dotted line corresponds to the mean of the observed and simulated losses.

The findings suggest that if 25 % of the cities had displayed a higher greenness index, losses from extreme rainfall in 2015 could have been reduced by approximately US\$ 6,500 million (2015 constant). This reduction accounts for roughly 19 % of the total estimated losses that year and a *t*-test confirms that the difference between the means of the distribution of observed and simulated losses is not equal to 0 (see Fig. 7).<sup>13</sup> This simulated scenario assumes the deployment of green infrastructure in 125 cities already displaying densely vegetated land cover, with a rise of the average greenness index of these cities from 13 % to close to 23 %.

Obviously, these results reflect the specific distribution of extreme rainfall events across cities during the year 2015 and could vary depending on the location, intensity and number of extreme rainfall events recorded over a year. Likewise, these estimates do not consider impacts which are not captured through NTL variations, such as human losses or natural capital degradation. They do, however, provide robust evidence of the benefits that green areas can generate for Latin American cities, in terms of avoided losses and reduced economic disruption generated by extreme rainfall.

## 5. Discussion and conclusion

This investigation provides empirical evidence that, in Latin America, the negative impact of extreme rainfall on urban economic activity is significantly reduced in cities displaying a greener land cover. These results were obtained using an internationally harmonised definition of cities and leveraging earth observations for the period 2013–2019. Urban economic activity was proxied using monthly night-time lights. Extreme rainfall was detected through an analysis of precipitation patterns over 30 years and the greenness of the land cover was categorised using NDVI composites. To measure the impact of extreme rainfall on urban economic activity, a fixed effects model was employed to control for unobserved city heterogeneity and common monthly changes to all cities in each country. Then, to examine the extent to which the impact of extreme rainfall is differentiated across cities, an interaction term, based on the share of green areas detected within city boundaries, was introduced. Eventually, a counterfactual analysis for the year 2015 was

conducted and suggested that if 25 % of the cities in our sample had increased their average share of green land cover to above 20 %, an additional US\$ 6,500 million could have been reaped, in terms of avoided losses and reduced disruption. Taken together, these findings reveal how a more balanced land cover, which makes room for green infrastructure within the city, can contribute to shield economic activity from adverse effects associated with extreme rainfall.

While most of the previous studies assessing the role of GI for flood protection relied on hydrological modelling at the watershed level, the methodology used in this paper innovates in at least two major dimensions: (i) it relies on empirical observations to measure extreme rainfall impacts (as opposed to modelling a set of synthetic flood events); and (ii) it covers a much larger geographical area, spanning nine years of rainfall observations. Consequently, findings differ from those obtained through hydrological modelling studies and do not offer tailored recommendations about the design and location of urban GI at the watershed level.

Instead, the proposed investigation focuses on providing robust evidence that, for most intermediate and small cities in Latin America, a greener land cover can alter the impacts of extreme rainfall. This framework provides a solid methodology to quantify the benefits delivered by GI in terms of avoided losses or reduced economic disruption in case of extreme rainfall. This adds further evidence on the multiple ecosystemic services provided by GI (e.g. improved air and water quality, temperature regulation, enhanced biodiversity or recreational opportunities, among others) and contributes to expand the methods that can be mobilized to quantify these services. Ultimately, by contributing to a sound quantification of the wide-ranging benefits associated with GI, this study seeks to inform urban public policies about the strategic value of these interventions.

As cities continue to expand in flood prone areas and climate change further intensifies the hydrological cycle, more frequent and intense extreme rainfall events are expected to affect Latin American cities. This will only make the benefits associated with green infrastructure more relevant and should encourage future research on the efficacy and adequacy of GI for flood protection. Research at a finer spatial resolution will notably be required to examine how GI efficacy can be altered by the type of vegetation used or by different storm intensity and duration parameters under a changing climate. Due to the nature of the data used in this investigation, these factors have not been addressed but remain an important avenue for future investigations.

This research has been carried out as part of the Grant “Challenges,

<sup>13</sup> Observed losses for 2015 account for roughly 0.77% of the GDP of the 7 countries of interest, with the reduction in impact due to the higher greenness accounting for 0.15% of the aggregated GDP.

discoveries and opportunities in post pandemic Economic Geography: the workspace, the mobility and the public space in Barcelona” funded by MCI/AEI/ PID2020-112734RB-C32.

**CRedit authorship contribution statement**

**Rafael Van der Borcht:** Writing – original draft, Visualization, Validation, Software, Methodology, Investigation, Formal analysis, Data curation, Conceptualization. **Montserrat Pallares-Barbera:** Writing – review & editing, Supervision, Resources, Project administration, Methodology, Funding acquisition, Conceptualization.

**Declaration of competing interest**

The authors declare that they have no known competing financial interests or personal relationships that could have appeared to influence the work reported in this paper.

**Data availability**

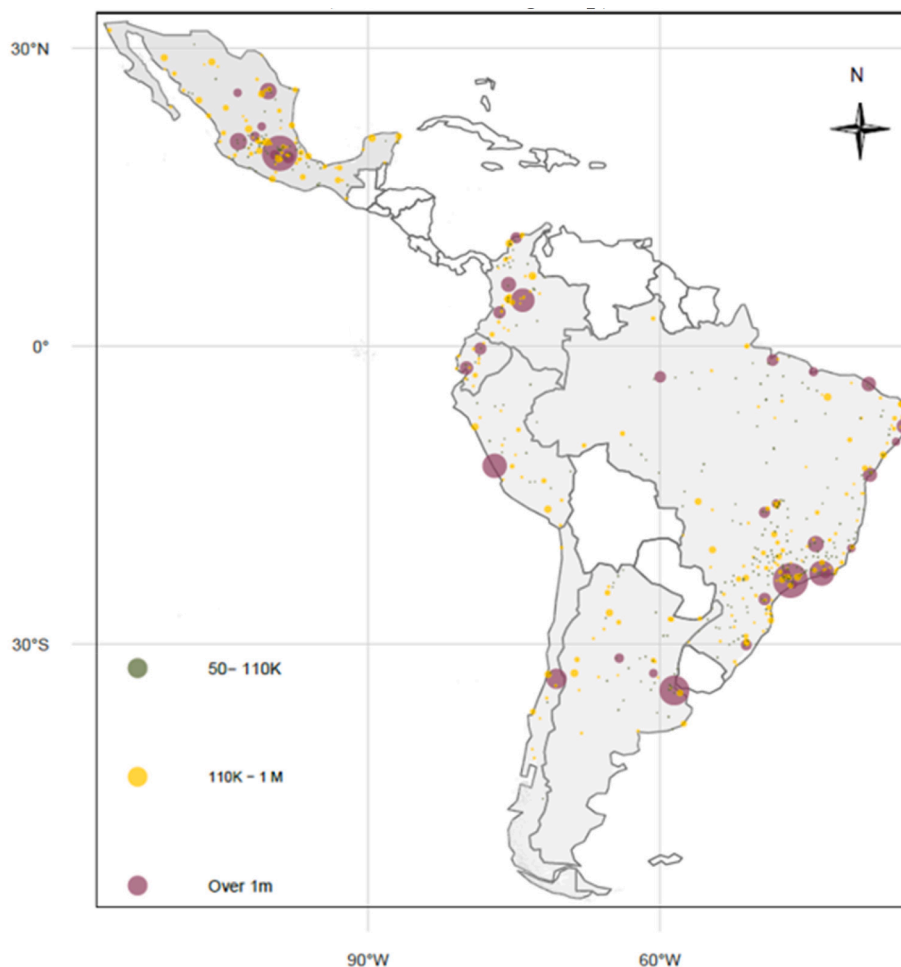
Data will be made available on request.

**Appendix A. City-level statistics and spatial distribution**

**Table A.1**  
Summary statistics.

Variable	Mean	Std. Dev.	Min	Max
Ln NTL/cap	7.8	1.3	-6.9	10.7
Extreme Precipitation*	2.6	0.5	2	5.3
Greenness index	0.4	0.2	0.1	1.0

\*Extreme precipitation statistics were only computed for realised events, i.e. excluding observations where the index was equal to 0.



Note: The size of the bubble is proportional to the population of the city in 2015  
Source: UCDB

**Map A.1.** Spatial distribution and population (in 2015) of the cities included in the study. Note: The size of the bubble is proportional to the population of the city in 2015. Source: UCDB.

**Appendix B. Robustness checks**

Extensive robustness checks were conducted to test the sensitivity of the results to different assumptions and specification choices. First, we altered the sample of cities by including all cities detected in the seven countries of interest, i.e. not restricting our sample to cities that have experienced at least one extreme rainfall event over the period of analysis. This raised the number of cities from 630 to 736 but did not substantially modify the results. [Table B.1](#) follows the same approach that the main results displayed in [Table 1, Section 4](#). It shows how the extreme rainfall index (columns 1–2), the above average precipitation value (column 3) and the full scope of Z-score values attached to monthly precipitation (columns 4–5) all have a negative impact on the NTL/cap at the city-level of a similar magnitude to those observed with the restricted sample of cities. When considering this broader sample of cities, the only difference with baseline results appears in column 4, which seems to suggest that there is a U-shaped relationship between precipitation Z scores and the NTL/cap. However, the vertex of this curve is reached with a Z score of 4.78, which is very close to the maximum value of the sample and would imply a potential positive impact on NTL/cap for only a handful of observations. We further tested the sensitivity of our results by removing cities in Brazil, which represented almost half of the cities in our sample, before estimating Eq. (4) with the three aforementioned precipitation indexes. The results remain consistent and suggest a statistically significant negative impact, although a bit noisier and of a lower magnitude (between  $-0.037$  and  $-0.023$ ).

**Table B.1**  
Sensitivity of results to altering the sample of cities by including cities that did not experience extreme rainfall events over the period.

	Dependent variable: Ln NTL/cap				
	(1)	(2)	(3)	(4)	(5)
Xtrm Rainfall	-0.076*** (0.014)	-0.085*** (0.014)			
Rainfall Zscore				-0.067*** (0.007)	-0.059*** (0.005)
Sq. Rainfall Zscore				0.007** (0.003)	
Temp. Z	0.059*** (0.005)			0.046*** (0.005)	0.047*** (0.005)
Sq. Temp. Z	-0.016*** (0.004)			-0.017*** (0.004)	-0.016*** (0.004)
Abov. mean rainfall			-0.085*** (0.008)		
Observations	80,352	80,352	80,352	80,352	80,352
F Statistic	60.009*** (df = 3; 79390)	65.545*** (df = 1; 79392)	151.218*** (df = 1; 79392)	67.789*** (df = 4; 79389)	88.436*** (df = 3; 79390)

Note: \*p < 0.1; \*\* p < 0.05; \*\*\* p < 0.01.

Additionally, we changed the structure of our fixed effects by using a subregional-monthly time trend (i.e. a South America-Monthly and Central America-Monthly fixed-effect as opposed to a country-monthly time trend), with little difference in magnitude or significance for the coefficients of interest ([Table B.2](#)). Simple monthly fixed effects for the entire continent were also used and delivered consistent results. The use of a month-by-province time trend was not tested as it would dramatically increase the number of fixed-effects (by 23,868 corresponding to 221 provinces\* 108 months), strongly reducing the variance in our data and obscuring the statistical effects of our variable of interest. Finally, we computed standard errors using a two-way clustering (i.e. city and country-monthly or subregional-monthly clustering) and confirmed that this did alter the significance of our results.

**Table B.2**  
Sensitivity to changing the structure of the time trend to subregional-monthly fixed-effects.

	Dependent variable: Ln NTL/cap				
	(1)	(2)	(3)	(4)	(5)
Xtrm Rainfall	-0.079*** (0.014)			-0.087*** (0.014)	
Rainfall Zscore		-0.065*** (0.006)	-0.070*** (0.007)		
Sq. Rainfall Zscore			0.004 (0.003)		
Temp. Z	0.060*** (0.006)	0.046*** (0.005)	0.045*** (0.005)		
Sq. Temp. Z	-0.013*** (0.004)	-0.013*** (0.004)	-0.014*** (0.004)		
Abov. mean rainfall					-0.093*** (0.009)
Observations	68,040	68,040	68,040	68,040	68,040
F Statistic	75.746*** (df = 3; 67192)	116.469*** (df = 3; 67192)	87.970*** (df = 4; 67191)	96.940*** (df = 1; 67194)	219.199*** (df = 1; 67194)

Note: \*p < 0.1; \*\* p < 0.05; \*\*\* p < 0.01.

Eventually, we included a lagged extreme rainfall index and confirmed that the contemporaneous effect associated with extreme rainfall remains significantly negative and of a magnitude similar to the one estimated previously (see column 1 in [Table B.3](#)). A very similar pattern is observed when using rainfall above the mean (column 2 in [Table B.3](#)) or precipitation z-score and their lagged versions.

**Table B.3**  
Time dimension of the extreme rainfall index (col 1) and of Z scores values above 0 (col 2).

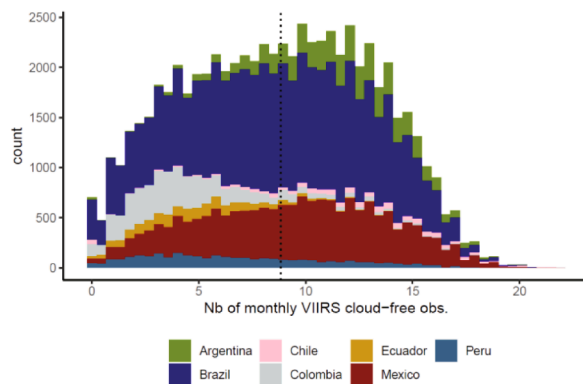
	Dependent variable:	
	Ln NTL/cap	
	(1)	(2)
Xtrm Rainfall	−0.09 <sup>***</sup> (0.020)	
Lag xtrm	−0.02 (0.010)	
Lag2 xtrm	0.01 (0.010)	
Lag3 xtrm	−0.01 (0.010)	
Lag4 xtrm	−0.01 (0.010)	
Lag5 xtrm	0.01 (0.010)	
Lag6 xtrm	0.02 <sup>**</sup> (0.010)	
Above norm.		−0.09 <sup>***</sup> (0.020)
Lag abv norm		−0.02 (0.010)
Lag2 abv norm		0.01 (0.010)
Lag3 abv norm		−0.02 <sup>*</sup> (0.010)
Observations	64,260	66,150
F Statistic	15.61 <sup>***</sup> (df = 7; 63420)	59.75 <sup>***</sup> (df = 4; 65307)

Note: \*p < 0.1; \*\* p < 0.05; \*\*\* p < 0.01.

### Appendix C. Cloud-free coverage

As mentioned in the main text and in [Elvidge et al. \(2017\)](#), varying cloud coverage quality can influence the value of monthly VIIRS NTL. For our sample of NTL values aggregated at the city-level, VIIRS NTL values are based on an average of 9 days of cloud-free coverage per month. Although the distribution of cloud-free observations varies across the seven countries of interest, they all follow a similar pattern and display a limited number of observations with 15 or more cloud-free days ([Histogram C.1](#)). When looking at the average number of cloud-free observations by month over the period 2013–2021, a seasonal pattern can be detected: Brazil and Peru experienced a notable increase in the number of cloud-free observations during April to September, while it seems to be the inverse in Mexico and, to a lesser extent, in Chile (see [Histogram C.2](#)). Argentina is the only country where the number of cloud-free observations is flat all year round, at approximately 10 days/month, which is why Argentina is not included in [Histogram C.2](#). Importantly, the average value of city NTL/cap seems to follow this seasonal trend but with less pronounced variations: higher (or lower) NTL values are recorded during the months where more (or less) cloud-free observations are available. Overall, with a Pearson's coefficient estimated at 0.32, the correlation between cloud-free observations and NTL values is quite strong and warrants a cautious approach. In this setting, the observed reduction in NTL values during months of high cloud-coverage (which are also the months where extreme rainfall events tend to occur) could confound the estimation of extreme rainfall impact.

As argued in the main text, the inclusion of a country-monthly fixed effect in Eq. (4) allows the soaking up of all the monthly variations in cloud coverage, that commonly affects the NTL values of cities within a given country. As cloud coverage is more spatially diffuse than extreme rainfall, which are by nature very localized events, we consider that this country-monthly fixed effects at least partially limit this issue. However, to further control the potential impact of cloud coverage variations we used two additional robustness tests. First, we used a more restrictive cloud-coverage quality threshold and removed cities that had less than 6 days of cloud-free observations, on average (i.e. almost a quarter of the sample, or 88 cities, were removed), with the objective of excluding these cities, which are regularly affected by high cloud coverage from the estimation. Second, we added an additional quarter trend fixed effect, to capture a potential cyclical winter/summer variation due to cloud coverage. The results of these two estimations are shown in column 1 and 2 of [Table C.1](#), respectively, and confirm our previous results: extreme rainfall events have a negative impact on city NTL/cap that does not seem to be driven by lower cloud-free observations.

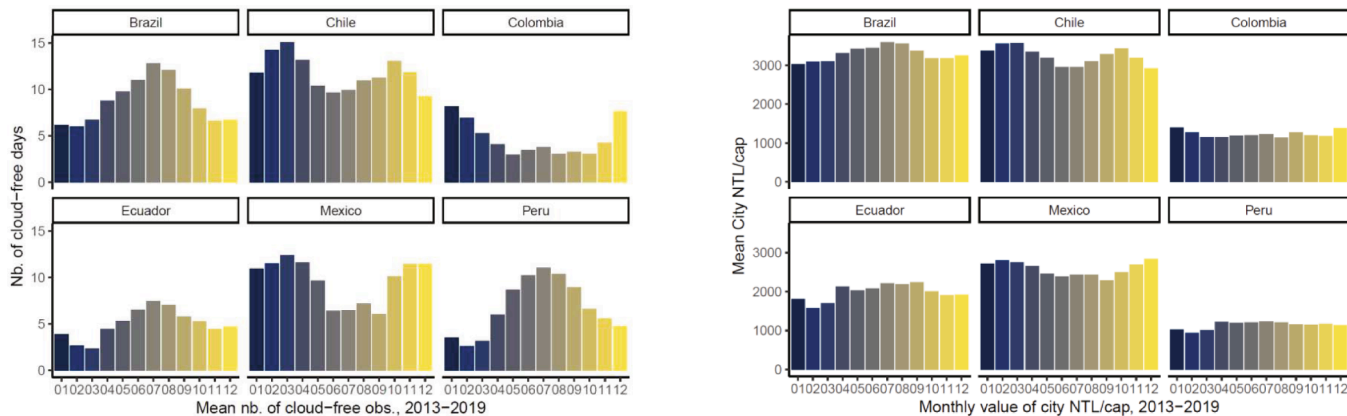


**Histogram C.1.** Number of cloud-free observations used to compute the monthly NTL values, 2013-2021.

**Table C.1**  
Results for additional cloud coverage quality controls.

	Dependent variable: Ln NTL/cap	
	(1)	(2)
Xtrm Rainfall	-0.058*** (0.012)	-0.079*** (0.014)
Temp. Z	0.046*** (0.005)	0.060*** (0.006)
Sq. Temp. Z	-0.014*** (0.003)	-0.013*** (0.004)
Observations	58,536	68,040
F Statistic	56.503*** (df = 3; 57776)	75.746*** (df = 3; 67192)
Restrictive cloud-coverage quality threshold (>6 days)	YES	NO
Additional Quarter fixed-effect	NO	YES

Note: \*p < 0.1; \*\* p < 0.05; \*\*\* p < 0.01.



**Histogram C.2.** Monthly distribution of mean cloud-free observations (left) and NTL values (right), 2013-2021.

**Appendix D. Greenness index sensitivity analysis**

To test the sensitivity of our results to different greenness index specifications, we conducted extensive robustness checks. First, we altered the different NDVI and greenness index thresholds values used in the main text. Specifically, we started by estimating Eq. (5) including all cities with a greenness index above 1. In doing so, we added 93 cities to the sample used in the main text, which included all cities with a greenness index higher than 5. To ease comparisons, column 1 of in Table D.1 reports the results for our benchmark model using the sample of cities from the main text. Following columns report results splitting the larger alternative sample into two groups at the values corresponding to the median (col. 2) and the 3rd tercile of the greenness index (col. 3). Results confirmed that a higher greenness index reduces the negative effects of extreme rainfall events. Interestingly, the model based on the median value of this new sample (i.e. a greenness index of 13.45) suggests that the difference of impacts between the two bins is not statistically significant, while the model based on the third tercile (i.e. a greenness index of 20.31) evidences a significant difference

in impacts, with a reduction of a similar magnitude to what was obtained using the sample in the main text. These estimates suggest that, on average, cities with a greenness index higher than 20 display a lower vulnerability to extreme rainfall events. Results varying the minimum greenness index threshold between 1 and 5 suggested a consistent pattern but are not reported, for the sake of conciseness.

**Table D.1**  
Econometric results for different greenness index threshold.

	Dependent variable: Ln NTL/cap		
	(1)	(2)	(3)
Xtrm Rainfall	-0.120*** (0.031)	-0.085*** (0.024)	-0.093*** (0.019)
Xtrm Rainfall: Med. Greenness	0.064* (0.033)	0.009 (0.030)	
Xtrm Rainfall: 3rd Quart. Greenness			0.049** (0.024)
Observations	54,324	64,368	64,368
F Statistic	37.282*** (df = 2; 53064)	36.500*** (df = 2; 63015)	39.185*** (df = 2; 63015)
Minimum greenness index value	5	1	1

Note: \*p < 0.1; \*\*p < 0.05; \*\*\*p < 0.01.

We then considered a NDVI threshold value of 0.6 to categorize pixels as “dense vegetation pixels” (as opposed to a NDVI threshold value of 0.5 in the main text) and repeated the estimation strategy employed above. **Table D.2** reports the results of this more restrictive NDVI threshold value, considering cities displaying a greenness index above 5. Results confirm that previous findings hold, although the difference in effects between the different bins is only statistically different for the model splitting the sample at the 4th quartile of the greenness index (col. 3).

**Table D.2**  
Econometric results using a NDVI threshold of 0.6 to define dense vegetation pixels.

	Dependent variable: Ln NTL/cap		
	(1)	(2)	(3)
Xtrm Rainfall	-0.113*** (0.029)	-0.106*** (0.024)	-0.104*** (0.022)
Xtrm Rainfall: Med. Greenness	0.046 (0.033)		
Xtrm Rainfall: 3rd Tercile Greenness		0.045 (0.029)	
Xtrm Rainfall: 4th Quart. Greenness			0.058** (0.028)
Observations	42,660	42,660	42,660
F Statistic (df = 2; 41508)	41.638***	41.277***	41.977***
NDVI Threshold Value	0.6	0.6	0.6

Note: \*p < 0.1; \*\*p < 0.05; \*\*\*p < 0.01.

Eventually, we removed cities with a very high greenness index (i.e. cities with a greenness index above 40) to ensure that the estimated effects did not depend on a few cities that could be viewed as outliers, in terms of land cover. Results are almost identical to these displayed in column 1 of **Table D.1** and confirm that previous results are not overly sensitive to these high values.

A second set of robustness checks tested an alternative NDVI spatiotemporal resolution. To this end, we leveraged the dataset provided by [Corbane et al. \(2020\)](#), which computed NDVI values within urban centers using the same underlying Landsat annual composites, but working at a 1 km resolution on a time interval that spans from 2012 to 01-01 to 2015–12-30 i.e. only the first part of the period considered in the analysis. Resulting pixel values were classified into one of the three classes as follows: values below 0.1 are associated with built-up structures, barren rock, sand or snow; pixel values in between 0.2 and 0.5 are assumed to correspond to shrubs or agriculture areas; pixel values above 0.6 are associated with dense vegetation such as forests, urban garden or parks. We used these categorical values to compute our greenness index as the ratio of pixels above 0.6 over all city pixels, in a similar fashion to our greenness index shown in Eq. (3) in **Section 2** of the main text.

Results are shown in **Fig. D.1** following the same structure than in the main report: the city greenness index has been discretized into various bins corresponding to the q-quantile values of this alternative greenness index. Again, to exclude any protection benefits that could be derived from the fact that cities without dense vegetation are intrinsically more vulnerable to extreme rainfalls, we excluded cities with a greenness index below 0.1 (approximately 10 % of cities from our original sample). We find that differences in impacts are particularly visible when splitting cities into three bins. In this model, for cities below the third tercile of greenness, the marginal extreme rainfall effect reduces nightlights by more than 10 %. Contrastingly, in cities with greenness indexes above the third tercile (with an average green index of 0.66), this marginal effect is reduced to approximately -5 %. In addition, we tested and rejected the null hypothesis of no differential impact of extreme rainfall events between the second and third bins (P value < 0.1). Models with q = 4 and q = 2 show a consistently decreasing impact of extreme rainfall, as the level of greenness increases. In the case of the q = 4 model, we were able to reject the null hypotheses of equality between the coefficients associated with the last bin and the second bin (P value < 0.1). However, we were not able to reject it for the model with q = 2 at conventional levels. Overall, when using this alternative source of data, the estimated impacts suggest that adverse effects triggered by extreme rainfall are attenuated in a similar magnitude than previously estimated, although effects seem a bit noisier with this coarser spatial resolution.

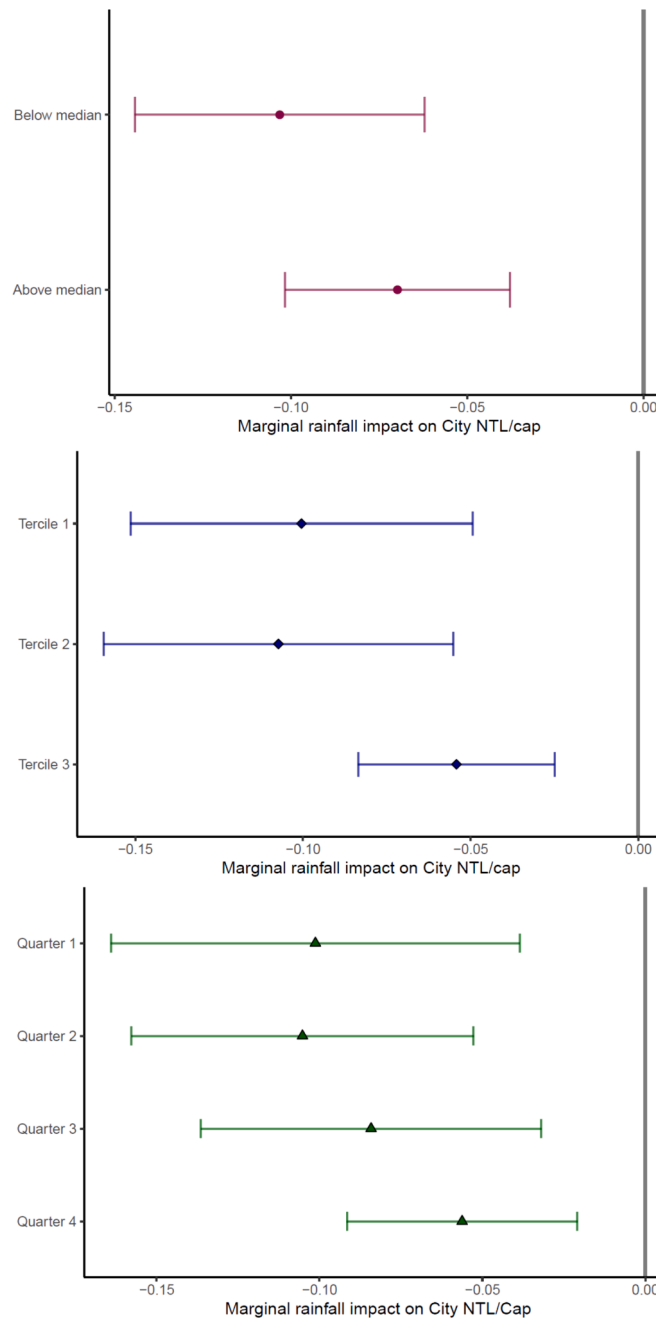


**Fig. D.1.** Estimated effects of three models of extreme rainfall interacting with q-quantiles of greenness index ( $q = 2$ ,  $q = 3$  and  $q = 4$ ) using NDVI values from Corbane et al. (2020).

Although this investigation has focused on the greenness of the land cover, the effect of extreme rainfall on city NTLs may differ along many dimensions. To ensure that the differentiated impacts reported above are not driven by other sources of heterogeneity potentially correlated to the greenness index, we have performed a final set of robustness checks. Three additional source of heterogeneity that could have potentially confounded our estimation were considered: the population of a city, the mean precipitation level and its elevation. We therefore used Eq. (5) in the main text and interacted our extreme rainfall variables with the greenness index as well as a new interaction term based on either (i) 2015 city population, (ii) average rainfall over the period 2013–2021 or (iii) the average elevation of each city.

The population of a city might constitute a very important dimension likely to shape extreme rainfall impacts on city NTLs. We posit that the more populated the city, the lower the marginal impact of extreme rainfall events. In fact, for the largest cities in our sample, due to scale effects, it is unlikely that a given extreme rainfall event affects the entire city population. NTL reductions in one area might thus have a modest impact on overall city NTLs or might even be compensated by positive effects in another area of the city. For very large cities, these spatial spillovers could “averaged out” extreme rainfall effects and produce unclear aggregated effects on city NTLs.

Extreme rainfall effects might also be differentiated in wet and dry regions. We assume that wet regions are used to deal with abundant rainfall and might have more incentives to invest in infrastructure that limit surface run-off and channel water out of the city. In other words, cities in wet regions might be better equipped to cope with extreme rainfall events than cities in dry regions, where rainfall is low and concentrated only over a few months of the year. Although this dimension is partially captured in the z-score formula used to depict extreme rainfall events, we used this second interaction

term to test for this effect more explicitly.

Finally, extreme rainfall effects might also be moderated by the elevation of a city. One might expect that impacts of extreme rainfall will be more severe the further downstream a city is located because it is potentially located in areas more prone to flood risk and because pluvial flooding tends to be more intense downstream. Contrastingly, city located upstream or at higher locations could potentially experience less pronounced impacts because extreme rainfall will be more easily channelled out of the city. To test this effect, we have extracted the average elevation estimated within the extent of each city provided by the UCDB. This elevation is expressed in metres above sea level. Cities covered in sample range from almost sea-level altitude for coastal cities, to above 2,500 m for the highest cities in Peru, Colombia and Ecuador.

Results are shown in Table D.3 and confirm that the marginal effect of extreme rainfall is significantly reduced for cities displaying a higher than median greenness index, even considering these additional sources of heterogeneity. Column 1 indicates that adverse effects are diminished as city population increases, confirming that more populated cities tend to be less vulnerable to extreme rainfall. On the other hand, in column 2, the coefficient associated with average precipitation is not significant, suggesting that cities located in wet or dry regions do not display differentiated responses to extreme rainfall events, everything else being equal.<sup>14</sup> Finally, column 3 indicates that the higher the elevation of the city, the lower the negative effects associated with the extreme rainfall index, although this does not alter the benefits of a greener land cover.

**Table D.3**  
Other sources of heterogeneity potentially confounding the differentiated impacts of greenness.

	Dependent variable: Ln NTL/cap		
	(1)	(2)	(3)
Xtrm Rainfall	-0.568*** (0.202)	-0.123*** (0.032)	-0.150*** (0.038)
Xtrm: Greenness	0.074** (0.035)	0.064* (0.033)	0.067** (0.033)
Xtrm: Ln City Pop	0.037** (0.015)		
Xtrm: Av. Precip.		0.00001 (0.000)	
Xtrm: Elevation			0.0001*** (0.000)
Observations	54,324	54,324	54,324
F Statistic (df = 3; 53063)	29.324***	25.047***	29.228***

Note: \*p < 0.1; \*\* p < 0.05; \*\*\* p < 0.01.

Taken together, these robustness checks confirmed that the results presented in the main text were not driven by other sources of heterogeneity across our sample of cities, nor overly sensitive to the thresholds values employed to characterize city greenness or city outliers in terms of greenness index. Overall they increase our confidence in the estimates used in the main text.

**Appendix E. NTL vs GDP**

To estimate GDP variation associated with a given change in city NTL, we first need to compute national-annual NTL values from the city-monthly NTL sample we are using. To this end, we used the monthly NTL values to first calculate the mean annual NTL value for each city. We then summed annual city NTL values at a national level and regressed these values against the GDP values of each country, expressed in 2015 US\$ constant and extracted from the World Development Indicators of the World Bank. We first used a linear regression (column 1 of Table E.1) and then included a yearly fixed effect with a log-log relationship (column 2). In both cases, the coefficient of interest is highly significant and with a squared R above 0.90, estimations are deemed robust enough to provide a conversion factor. To illustrate this, Fig. E.1 plots the predicted GDP against the actual GDP values using the regression for column 1. As can be observed, all points are located close to the 45° line, revealing that NTL quite accurately predict GDP values. Consequently, we used the coefficient of column 1 to reproduce the simulation and counterfactual analysis presented in Section 4. This regression is by no means intended to be interpreted as a causal relationship, it simply seeks to establish a conversion factor between national city NTLs and GDP.

**Table E.1**  
The relationship between NTL and GDP.

	Dependent variable:	
	GDP OLS	Ln GDP panel linear
	(1)	(2)
Yearly NTL	42.99*** (1.550)	
Ln Yearly NTL		0.89*** (0.030)

(continued on next page)

<sup>14</sup> This is consistent with the results displayed in Column 4 of Table 1 of Section 3 in the main text, indicating that relationship between NTL and precipitation is not adequately captured by a U-shaped curve. It.

Table E.1 (continued)

	Dependent variable:	
	GDP OLS	Ln GDP panel linear
	(1)	(2)
Observations	63	63
R <sup>2</sup>	0.93	0.94
Adjusted R <sup>2</sup>	0.92	0.93
F Statistic	764.49*** (df = 1; 61)	806.75*** (df = 1; 53)

Note: \*p < 0.1; \*\* p < 0.05; \*\*\* p < 0.01.

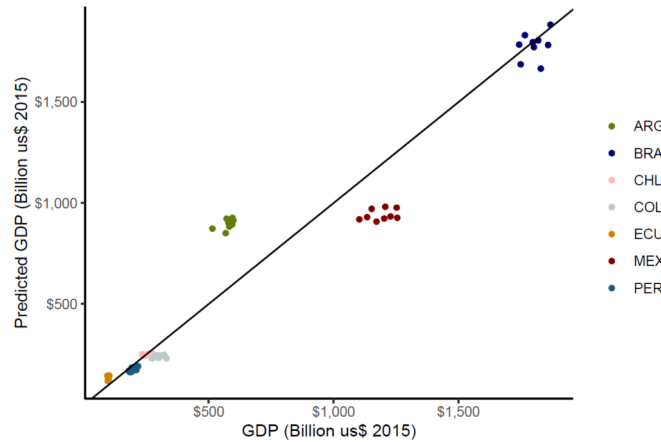


Fig. E.1. Predicted GDP using city-level NTL vs actual GDP, 2013–2021.

References

Anni, A.H., Cohen, S., Praskievicz, S., 2020. Sensitivity of urban flood simulations to stormwater infrastructure and soil infiltration. *J. Hydrol.* 588: 125028, ISSN 0022-1694. <https://doi.org/10.1016/j.jhydrol.2020.125028>.

Arnold, C.L., Gibbons, C.J., 1996. Impervious surface coverage: the emergence of a key environmental indicator. *J. Am. Plann. Assoc.* 62 (2), 243–258. <https://doi.org/10.1080/01944369608975688>.

Bhattacharjee, K., Behera, B., 2018. Does Forest cover help prevent flood damage? Empirical evidence from India. *Global Environ. Change* 53, 78–89, ISSN 0959-3780, <https://doi.org/10.1016/j.gloenvcha.2018.09.004>.

Brakenridge, G.R., 2023. Global Active Archive of Large Flood Events. Dartmouth Flood Observatory, University of Colorado, USA. <http://floodobservatory.colorado.edu/Archives/> (accessed august 21 2023).

Brink, E., Aalders, T., Ádám, D., et al., 2016. Cascades of green: a review of ecosystem-based adaptation in urban areas. *Global Environ. Change* 36, 111–123, ISSN 0959-3780. <https://doi.org/10.1016/j.gloenvcha.2015.11.003>.

Centre for Research on the Epidemiology of Disasters (CRED), 2015. EM-DAT: The CRED/OFDA International Disaster Database. Université Catholique de Louvain, Brussels, Belgium. <https://www.emdat.be> (accessed June 16, 2023).

Chen, X., Nordhaus, W., 2011. Using luminosity data as a proxy for economic statistics. *Proc. Natl. Acad. Sci. U.S.A.* 108(21), 8589–8594. <https://doi.org/10.1073/pnas.1017031108>.

Chen, X., Nordhaus, W., 2015. A test of the new VIIRS lights data set: population and economic output in Africa. *Remote Sens. (Basel)* 7, 4937–4947. <https://doi.org/10.3390/rs70404937>.

Corbane, C., Pesaresi, M., Politis, P., Florczyk, J.A., Melchiorri, M., Freire, S., Schiavina, M., Ehrlich, D., Naumann, G., Kemper, T., 2020. The grey-green divide: multi-temporal analysis of greenness across 10,000 urban centres derived from the Global Human Settlement Layer (GHSL). *Int. J. Digital Earth* 13 (1), 101–118. <https://doi.org/10.1080/17538947.2018.1530311>.

del Valle, A., de Janvry, A., Sadoulet, E., 2020. Rules for recovery: impact of indexed disaster funds on shock coping in Mexico. *Am. Econ. J. Appl. Econ.* 12 (4), 164–195. <https://doi.org/10.1257/app.20190002>.

del Valle, A., Erikssona, M., Ishizawa, O.A., Miranda, J.J., 2019. Mangroves protect coastal economic activity from hurricanes. *Proc. Natl. Acad. Sci. U.S.A.* 117(1), 265–270. <https://doi.org/10.1073/pnas.1911617116>.

Dell, M., Jones, B.F., Olken, B.A., 2014. What do we learn from the weather? The new climate-economy literature. *J. Econ. Lit.* 52 (3), 740–798. <https://doi.org/10.1257/jel.52.3.740>.

Dijkstra, L., Florczyk, A.J., Freire, S., Kemper, T., Melchiorri, M., Pesaresi, M., Schiavina, M., 2020. Applying the degree of urbanisation to the globe: a new

harmonised definition reveals a different picture of global urbanisation. *J. Urban Econ.*, 103312 <https://doi.org/10.1016/j.jue.2020.103312>.

Dottori, F., Szweczyk, W., Ciscar, J.C., et al., 2018. Increased human and economic losses from river flooding with anthropogenic warming. *Nat Clim Change* 8, 781–786. <https://doi.org/10.1038/s41558-018-0257-z>.

Du, S., Scussolini, P., Ward, P.J., et al., 2020. Hard or soft flood adaptation? Advantages of a hybrid strategy for Shanghai. *Global Environ. Change* 61, 102037, ISSN 0959-3780. <https://doi.org/10.1016/j.gloenvcha.2020.102037>.

Ellison, D., Morris C.E., Locatelli B., et al., 2017. Trees, forests and water: cool insights for a hot world. *Global Environ. Change* 43, 51–61, ISSN 0959-3780. <https://doi.org/10.1016/j.gloenvcha.2017.01.002>.

Elvidge, C.D., Kimberly, B., Mikhail, Z., Feng, C.H., Tilottama, G., 2017. VIIRS night-time lights. *Int. J. Remote Sens.* 38, 5860–5879. <https://doi.org/10.1080/01431161.2017.1342050>.

Felbermayr, G., Gröschl, J., Sanders, M., Schippers, V., Steinwachs, T., 2022. The economic impact of weather anomalies. *World Develop.* 151, 105745 <https://doi.org/10.1016/j.worlddev.2021.105745>. ISSN 0305–750X.

Florczyk, A., Corbane, C., Schiavina, M., Pesaresi, M., Maffeni, L., Melchiorri, M., Politis, P., Sabo, F., Freire, S., Ehrlich, D., Kemper, T., Tommasi, P., Airaghi, D., Zanchetta, L., 2019. GHS Urban Centre Database 2015, multitemporal and multidimensional attributes, R2019A. European Commission, Joint Research Centre (JRC). PID: <https://data.jrc.ec.europa.eu/dataset/53473144-b88c-44bc-b4a3-4583ed1f547e>.

Funk, C., Peterson, P., Landsfeld, M., et al., 2015. The climate hazards infrared precipitation with stations—a new environmental record for monitoring extremes. *Sci. Data* 2, 150066. <https://doi.org/10.1038/sdata.2015.66>.

Gibson, J., Olivia, S., Boe-Gibson, G., Li, C., 2021. Which night lights data should we use in economics, and where? *J. Develop. Econ.* 149: 102602, ISSN 0304-3878. <https://doi.org/10.1016/j.jdeveco.2020.102602>.

Gourevitch, J.D., Singh, N.K., Minot, J., Raub, K.B., Rizzo, D.M., Wemple, B.C., Ricketts, T.H., 2020. Spatial targeting of floodplain restoration to equitably mitigate flood risk. *Global Environ. Change* 61, 102050, ISSN 0959-3780. <https://doi.org/10.1016/j.gloenvcha.2020.102050>.

Güneralp, B., Güneralp, I., Liu, Y., 2015. Changing global patterns of urban exposure to flood and drought hazards. *Global Environ. Change* 31, 217–225, ISSN 0959-3780. <https://doi.org/10.1016/j.gloenvcha.2015.01.002>.

IPCC, 2023. Summary for Policymakers. In: *Climate Change 2023: Synthesis Report. Contribution of Working Groups I, II and III to the Sixth Assessment Report of the Intergovernmental Panel on Climate Change* [Core Writing Team, H. Lee and J. Romero (Eds.)]. IPCC, Geneva, Switzerland, pp. 1–34, doi:10.59327/IPCC/AR6-9789291691647.001.

Iungman, T., Cirach, M., Marando, F., Pereira, B.E., Khomenko, S., Masselot, P., Quijal-Zamorano, M., Mueller, N., Gasparri, A., Urquiza, J., Heris, M., Thondoo, M., Nieuwenhuijsen, M., 2023. Cooling cities through urban green infrastructure: a

- health impact assessment of European cities. *Lancet* 401 (10376), 577–589. [https://doi.org/10.1016/S0140-6736\(22\)02585-5](https://doi.org/10.1016/S0140-6736(22)02585-5).
- Jacobson, C.R., 2011. Identification and quantification of the hydrological impacts of imperviousness in urban catchments: a review. *J. Environ. Manage.* 92 (6), 1438–1448. <https://doi.org/10.1016/j.jenvman.2011.01.018>. ISSN 0301–4797.
- Jongman, B., Ward, P.J., Aerts, J.C.J.H., 2012. Global exposure to river and coastal flooding: Long term trends and changes. *Global Environ. Change* 22(4), 823–835, ISSN 0959-3780. <https://doi.org/10.1016/j.gloenvcha.2012.07.004>.
- Klomp, J., 2016. Economic development and natural disasters: a satellite data analysis. *Global Environ. Change* 36, 67–88, ISSN 0959-3780. <https://doi.org/10.1016/j.gloenvcha.2015.11.001>.
- Kocornik-Mina, A., McDermott, T.K., Michaels, G., Rauch, F., 2020. Flooded cities. *Am. Econ. J. Appl. Econ.* 12, 35–66. <https://doi.org/10.1257/app.20170066>.
- Lamond, J., Bhattacharya, N., Bloch, R., 2012. The role of solid waste management as a response to urban flood risk in developing countries, a case study analysis. *WIT Trans. Ecol. Environ.* 159, 193–204. <https://doi.org/10.2495/FRIAR120161>.
- Levin, N., Phinn, S., 2022. Assessing the 2022 flood impacts in queensland combining daytime and nighttime optical and imaging radar data. *Remote Sens.* 14, 5009. <https://doi.org/10.3390/rs14195009>.
- Mejía, A.L., Moglen, G.E., 2010. Spatial distribution of imperviousness and the space-time variability of rainfall, runoff generation, and routing. *Water Resour. Res.* 46 <https://doi.org/10.1029/2009WR008568>.
- Mohan, P., Strobl, E., 2017. The short-term economic impact of tropical cyclone pam: an analysis using VIIRS nightlight satellite imagery. *Int. J. Remote Sens.* 38, 5992–6006.
- Poussin J.K., Botzen W.W.J., Aerts J.C.J.H., 2015. Effectiveness of flood damage mitigation measures: Empirical evidence from French flood disasters. *Global Environ. Change* 31, 74–84, ISSN 0959 3780. <https://doi.org/10.1016/j.gloenvcha.2014.12.007>.
- Schmitt, T.G., Thomas, M., Etrich, N., 2004. Analysis and modelling of flooding in urban drainage systems. *J. Hydrol.* 299(3–4), 300–311, ISSN 0022-1694. <https://doi.org/10.1016/j.jhydrol.2004.08.012>.
- Schubert, J.E., Burns, M.J., Fletcher, T.D., Sanders, B.F., 2017. A framework for the case-specific assessment of green infrastructure in mitigating urban flood hazards. *Adv. Water Resour.* 108, 55–68, ISSN 0309-1708. <https://doi.org/10.1016/j.advwatres.2017.07.009>.
- Steinhausen, M., Paprotny, D., Dottori, F., Sairam, N., Mentaschi, L., Alfieri, L., Lüttke, S., Kreibich, H., Schröter, K., 2022. Drivers of future fluvial flood risk change for residential buildings in Europe. *Global Environ. Change* 76, 102559, ISSN 0959-3780. <https://doi.org/10.1016/j.gloenvcha.2022.102559>.
- Sun, Z., Du, W., Jiang, H., Weng, Q., Guo, H., Han, Y., Xing, Q., Ma, Y., 2022. Global 10-m impervious surface area mapping: a big earth data based extraction and updating approach. *Int. J. Appl. Earth Observ. Geoinf.* 109, 102800 <https://doi.org/10.1016/j.jag.2022.102800>. ISSN 1569–8432.
- Tabari, H., 2020. Climate change impact on flood and extreme precipitation increases with water availability. *Sci. Rep.* 10, 13768. <https://doi.org/10.1038/s41598-020-70816-2>.
- UNDRR, 2017. The GAR atlas: Unveiling global disaster risk. 2017 Global Assessment Report on Disaster Risk Reduction. United Nations Office for Disaster Risk Reduction, 129 p.
- Upreti, S., Cao, C., Gu, Y., Shao, X., 2017. Improving the low light radiance calibration of S-NPP VIIRS day/night band in the NOAA operations. In: 2017 IEEE International Geoscience and Remote Sensing Symposium (IGARSS), pp. 4726–4729.
- Van der Borgh, R., Pallares-Barbera, M., 2023. How urban spatial expansion influences CO2 emissions in Latin American countries. *Cities* 139, 104389. <https://doi.org/10.1016/j.cities.2023.104389>. ISSN 0264–2751.
- WMO, 2023. Guidelines on the Definition and Characterisation of Extreme Weather and Climate Events. World Meteorological Organization, WMO-No. 1310. Geneva.
- Yang, Y., Endreny, T., Nowak, D., 2015. Simulating the effect of flow path roughness to examine how Green infrastructure restores urban runoff timing and magnitude. *Urban For. Urban Green.* 14 (2), 361–367. <https://doi.org/10.1016/j.ufug.2015.03.004>.
- Yao, L., Wei, W., Chen, L., 2016. How does imperviousness impact the urban rainfall-runoff process under various storm cases? *Ecol. Indic.* 60, 893–905. <https://doi.org/10.1016/j.ecolind.2015.08.041>. ISSN 1470-160X.
- Zhao, N., Hsub, F., Cao, G., Samsond, E., 2017. Improving accuracy of economic estimations with VIIRS DNB image products. *Int. J. Remote Sens.* <https://doi.org/10.1080/01431161.2017.1331060>.
- Zhao, X., Yu, B., Liu, Y., Yao, S., Lian, T., Chen, L., Yang, C., Chen, Z., Wu, J., 2018. NPP-VIIRS DNB daily data in natural disaster assessment: evidence from selected case studies. *Remote Sens. (Basel)* 10, 1526. <https://doi.org/10.3390/rs10101526>.